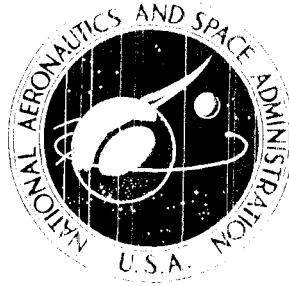


NASA CONTRACTOR  
REPORT



NASA CR-2681

NASA CR-2681

EFFECT OF GRAZING FLOW  
ON STEADY-STATE RESISTANCE  
OF ISOLATED SQUARE-EDGED ORIFICES

*Thomas Rogers and Alan S. Hersh*

*Prepared by*

HERSH ACOUSTICAL ENGINEERING

Chatsworth, Calif. 91311

*for Lewis Research Center*



NATIONAL AERONAUTICS AND SPACE ADMINISTRATION • WASHINGTON, D. C. • APRIL 1976

1. Report No. NASA CR-2681		2. Government Accession No.		3. Recipient's Catalog No.	
4. Title and Subtitle EFFECT OF GRAZING FLOW ON STEADY-STATE RESISTANCE OF ISOLATED SQUARE-EDGED ORIFICES				5. Report Date April 1976	
				6. Performing Organization Code	
7. Author(s) Thomas Rogers and Alan S. Hersh				8. Performing Organization Report No. None	
				10. Work Unit No.	
9. Performing Organization Name and Address Hersh Acoustical Engineering 9545 Cozycroft Avenue Chatsworth, California 91311				11. Contract or Grant No. NAS3-17858	
				13. Type of Report and Period Covered Contractor Report	
12. Sponsoring Agency Name and Address National Aeronautics and Space Administration Washington, D. C. 20546				14. Sponsoring Agency Code	
15. Supplementary Notes Final Report. Project Manager, Edward J. Rice, V/STOL and Noise Division, NASA Lewis Research Center, Cleveland, Ohio					
16. Abstract Steady-state diagnostic testing of an isolated orifice has shown the nature of the interaction between grazing and orifice flow causing the large increase in orifice resistance for both inflow and outflow. A simple inviscid interaction model has been developed which uses thin aerofoil theory to account for pressure forces exerted at the interface between the orifice and grazing flow together with a one-dimensional discharge coefficient concept. The effect of grazing flow boundary layer thickness was also included in the model. Resistance measurements for each orifice tested, over a wide range of grazing flow speeds and flow rates, collapse into a single curve when plotted in terms of effective discharge coefficient against orifice to grazing velocity ratio. The correlation curves for inflow and outflow are different. Data for clustered orifices collapse in the same way as those for the single orifice. The effect of boundary layer thickness is compared with model predictions. The correlation is of the form $C_{De} = \alpha (V_i/V_\infty)^n (\delta/D)^m$ where Resistance = $(1/2\rho) (V_i/C_{De})^2$ and $n \approx 1/2 \quad m \approx 1/10$ Orifice length-diameter ratio has no effect on resistance for outflow up to large orifice flow values ( $V_i/V_\infty \leq 0.5$ ), but has a significant influence at all orifice flow rates for inflow.					
17. Key Words (Suggested by Author(s)) Sound absorbers; Acoustic resistance; Nonlinear flow resistance; Orifice flow; Grazing flow			18. Distribution Statement Unclassified - unlimited STAR Category 71		
19. Security Classif. (of this report) Unclassified		20. Security Classif. (of this page) Unclassified		21. No. of Pages 58	22. Price* \$4.25

\* For sale by the National Technical Information Service, Springfield, Virginia 22161

## Table of Contents

	Page
1.0 INTRODUCTION	1
2.0 BACKGROUND	1
3.0 DIAGNOSTIC TESTING	3
3.1 Flow Visualization Testing	3
3.1.1 Flow Configuration During Outflow	4
3.1.2 Flow Configuration During Inflow	4
3.2 Instrumented Orifice Testing in a Wind Tunnel	4
4.0 THE INVISCID INTERACTION (LID) MODEL	5
4.1 Definitions and Assumptions	5
4.2 Lid Model Analysis for Outflow	6
4.3 The Lid Model for Inflow	8
4.4 Concluding Comments on the Lid Model Analysis	10
5.0 MEASUREMENTS OF STEADY STATE RESISTANCE OF SQUARE- EDGED ORIFICES IN GRAZING FLOW	10
5.1 Data Reduction	11
5.2 Test Results	12
5.2.1 Resistance Measurements at Low Orifice Flow Rates	13
5.2.2 Effects of Grazing Flow Boundary Layer Thickness	15
5.2.3 Effects of Orifice Length-Diameter Ratio	16
6.0 CONCLUSIONS	17
APPENDICES	
A Flow Regimes Observed in Water Tunnel	19
B Hersh Acoustical Engineering Wind Tunnel	21
C Instrumented Orifice Test Data	22

D	Extension of Lid Model to Circular Orifices	24
E	Discharge Coefficient of Orifices for Non-Grazing Flow	27
	SYMBOLS	28
	REFERENCES	29
	FIGURES	31

## SUMMARY

Steady State diagnostic testing of an isolated orifice has shown the nature of the interaction between grazing and orifice flow causing the large increase in orifice resistance for both inflow and outflow. A simple inviscid interaction model has been developed which uses thin aerofoil theory to account for pressure forces exerted at the interface between the orifice and grazing flow together with a one-dimensional discharge coefficient concept. The effect of grazing flow boundary layer thickness was also included in the model. Resistance measurements for each orifice tested, over a wide range of grazing flow speeds and flow rates collapse into a single curve when plotted in terms of effective discharge coefficient versus orifice to grazing velocity ratio. The correlation curves for inflow and outflow are different. Data for clustered orifices collapse in the same way as the single orifice. The effect of boundary layer thickness is compared with model predictions. The correlation is of the form

$$C_{De} = \alpha (V_i/V_\infty)^n (\delta/D)^m \quad \text{where}$$

$$\text{Resistance} = 1/2\rho V_i/C_{De}^2$$

$$\text{and } n \approx 1/2 \quad m \approx 1/10$$

Orifice length-diameter ratio has no effect on resistance for outflow up to large orifice flow values ( $V_i/V_\infty \leq 0.5$ ), but has a significant influence at all orifice flow rates for inflow.

## 1.0 INTRODUCTION

Sound absorbent linings consisting of cavity-backed perforated and/or porous faced lining materials are used for the control of internally generated machinery noise. Applied to the inlet and/or exhaust ducting of modern jet engines, the liner encounters high duct flow velocities and intense sound pressure levels, both of which strongly affect the local acoustic wall impedance.

It has been shown by Morse<sup>1</sup> and Cremer<sup>2</sup> (for a rectangular duct without flow) and by Rice<sup>3</sup> (for ducts with flow) that sound attenuation drops off sharply for off-optimum wall impedance. In aircraft, the amount of sound absorbent treatment is limited by aerodynamic and structural performance constraints, so it is critical to the effective and economical use of wall treatment that there be an accurate description of the wall impedance and a clear and detailed understanding of the parameters affecting it.

Zorumski and Parrott<sup>4</sup> showed experimentally and recently Hersh and Rogers<sup>5</sup> showed analytically (by establishing the quasi-steady nature of the flow in orifices exposed to intense sound levels) for the case of zero duct grazing flow, that the acoustic resistance of orifices is independent of frequency and that therefore, steady state (i.e., zero frequency) resistance measurements give a good approximation to acoustic resistance. A similar close connection, discussed by Groeneweg<sup>6</sup>, between steady state and acoustic resistance has been demonstrated by Plumblee et al.<sup>7</sup> Feder and Dean<sup>8</sup> and Armstrong<sup>9</sup> to exist even in grazing flow. Those studies demonstrated clearly the value and importance of studying the steady state behavior of orifices as a necessary prelude to understanding the physics of the acoustic behavior of orifices in grazing flow. Consequently the experimental and analytical study to be described herein was undertaken to clarify the physics of the effect of grazing flow on steady state orifice resistance as a first step in an ongoing effort to understand the acoustic behavior of orifices in grazing flow.

This report purports to show that steady state (and by implication, acoustic) orifice resistance data is best interpreted in terms of the classical concept of a discharge coefficient. It is shown, that interpreted or presented in this way, that a heretofore very complicated and confusing picture of the effects of grazing flow and other variables (orifice shape, boundary layer thickness, etc.) is greatly simplified, and that simplified modeling is possible.

## 2.0 BACKGROUND

Acoustic resistance measurements of orifices with grazing flow reported by Groeneweg<sup>6</sup> in a survey paper showed extreme sensitivity to both sound pressure level and grazing flow velocity (see also Plumblee<sup>7</sup> et al., Feder and Dean<sup>8</sup> and Armstrong<sup>9</sup>). Acoustic resistance increased with grazing flow speed for a constant sound pressure level. Similar behavior was observed for steady state resistance by Budoff and Zorumski<sup>10</sup>, who made a detailed

study of the steady state resistance of single and clustered orifices in a tangential (or grazing) flow.

Budoff and Zorumski showed that for low orifice flows (either inflow or outflow) resistance increased significantly with grazing flow velocity. In contrast, for large normal flows, very modest changes in flow resistance occurred for wide variations in grazing velocities. Similar results were obtained earlier by Feder and Dean<sup>8</sup> but no physical explanation of the spectacular effect of grazing flow was presented.

The effects of grazing flow on orifice resistance were studied earlier by Dittrich<sup>11</sup> and by Stokes<sup>12</sup> with reference to can combustor and boundary layer bleed technology and more recently in connection with the venting of launch and reentry vehicles<sup>13,14</sup>.

Goethert<sup>5</sup> summarizes an extensive amount of data for the inflow (flow into the wall - called outflow in this reference) case using the mass flow ratio ( $\rho V_i / \rho V_\infty$ ) and  $\Delta p / q_\infty$  correlating parameters.  $\Delta p$  and  $V_i$  are related naturally through discharge coefficient but this is not explicitly referred to. Dittrich and Stokes do interpret inflow resistance data in terms of discharge coefficient. They obtained an excellent correlation of data for a wide range of orifice size and grazing flow velocity similar to that presented herein (though the ideal orifice flow and therefore discharge coefficient is defined differently - total not static pressure in the grazing flow was used for orifice upstream pressure). Haukohl<sup>13</sup> presents a wide range of data using discharge coefficient but no general correlation was attempted. Neither did Walters<sup>14</sup> et al. generalize the extensive outflow data they presented. The launch and reentry vehicle venting data of these references, which covers up to the transonic range of  $V_i$  for both inflow and outflow cases shows the same general characteristic mentioned earlier (i.e. orifice resistance increases with increasing grazing flow velocity).

In early attempts to understand the effects of grazing flow on liners, Ingard<sup>16</sup> proposed that low frequency pressure fluctuations in the grazing flow (turbulent) boundary layer produced a resistance increase by superimposing additional rms velocity on the fluid moving through the liner as a result of the incident sound, the effect being similar to that produced by a steady bias velocity. Rice<sup>17</sup> pointed out that the large increase in orifice acoustic resistance due to grazing flow could not be accounted for by relying on boundary layer fluctuations. The amplitude was not high enough and the known effect of boundary-layer thickness was opposite to that predicted.

Sirignano<sup>18</sup> suggested for the outflow half of the acoustic cycle that an increase in velocity of the fluid leaving the orifice is induced by the reduced mean static pressure around the jet analogous to that which can be shown analytically for flow of an ideal fluid around a circular cylinder. The effect of this would be to decrease orifice resistance by increasing flow through the orifice ( $R = \Delta p / V$ ). This certainly is no explanation of the general effect

of grazing flow in increasing resistance but will be suggested later to explain a reduction in resistance (below the non-grazing flow value) that occurs for very high outflow rates (actually beyond the range of interest in jet engines -  $0.5 < V_i/V_\infty < 2.0$ ).

This report presents the results of diagnostic experiments consisting of flow visualization tests in a small water tunnel and lip static pressure data taken in a wind tunnel using a large (12.7 mm dia.) orifice which gave considerable insight into the effect of a grazing or tangential flow on flow into (inflow case) or out of (outflow case) a square-edged wall orifice. There follows a development of a simple inviscid interaction model where the interface between the grazing flow and the orifice flow is treated as a thin lid or membrane hinged at the upstream edge of the orifice for outflow and the downstream edge for inflow. Finally, steady state resistance data is presented for a wide range of variables and the correlation of the data is compared with the analytical (lid) model predictions.

### 3.0 DIAGNOSTIC TESTING

To give a better understanding of the physics of the effect of grazing flow on resistance, two kinds of simple diagnostic experiments were made. Flow visualization tests using dye were made in a small water tunnel and the qualitative results obtained were explored in more detail in a subsonic wind tunnel using a large 12.7 mm diameter orifice extensively instrumented with static pressure taps.

#### 3.1 Flow Visualization Testing

Because of the ease with which flow interaction effects can be made visible in water by injecting dye, a small transparent water tunnel was fabricated from a clear acrylic sheet and was connected to a water supply. The water tunnel is shown schematically in Figure 1 and described in Appendix A. The known effects of grazing flow in air occur where the flow rates in the orifice are low and the flow field may be assumed incompressible. The kinematic viscosity difference between air and water permits a Reynolds number simulation (based on hole diameter) using a 15-fold decrease in the duct flow velocity given the same orifice dimensions. Therefore, the Reynolds number of the water tunnel orifice (based on width of the rectangular orifice and the grazing flow velocity) during maximum duct flow conditions ( $V_\infty \approx 0.3$  m/sec) is in the range of practical interest for wall perforations in jet engines (where dia  $\sim 1 - 4$  mm, duct velocities  $\sim 100 - 300$  m/sec).

Five distinct flow regimes, shown schematically in Figure 2, were identified based on the relative flow rate and direction through the orifice. The characteristics of these interaction flow regimes are described in detail in Appendix A. The regimes are namely (1) The Zero Flow Regime, (2) The Low Outflow Regime, (3) The Low Inflow Regime, (4) The High Outflow Regime, and (5) The High Inflow Regime. The high flow regimes (4) and (5) are of

limited interest with respect to (aircraft) liner acoustics and will receive only cursory attention in this report. Attention is focused on the low flow regimes (2) and (3) and in particular on the characteristics of the dividing stream surface between the fluid passing over the orifice and that entering (for inflow case) or leaving (for outflow case) the orifice.

### 3.1.1 Flow Configuration During Outflow

In the absence of interpenetration or mixing of the two streams at the orifice opening (and it is easily shown that diffusion is negligible), the emerging fluid must interact with the grazing flow by deflecting it away from the mouth of the orifice. The deflected grazing flow in turn exerts drag on the orifice fluid turning and accelerating it in a downstream direction and at the same time providing an opening at the downstream edge of the orifice through which the fluid flows out of the orifice. The degree of opening is obviously a controlling factor in determining the resistance of the orifice. This is shown schematically in Figure 2(b). The dividing stream surface may be visualized as a drag interaction area and its deflection related to an effective orifice opening or flow area analogous to the classical concept of the "Vena Contracta". Later, the flow configuration described here will be incorporated in an analytical model.

### 3.1.2 Flow Configuration During Inflow

The grazing flow which is eventually captured by the orifice during inflow deflects and accelerates towards the opening and the dividing stream surface (between fluid entering the orifice and that passing on) impinges at the downstream lip of the orifice. Such a flow configuration is induced by the difference in pressure between the cavity and the grazing flow moving by the wall. This difference may be induced during the duration of the compression half of a sound wave ( $\lambda \gg D$ ) or in the steady state analog by creating a pressure drop in the cavity relative to the grazing flow pressure. Whereas during outflow the orifice is filled with fluid, this is not the case for inflow. Grazing flow entering the orifice separates from the upstream lip and is deflected into the orifice. For low inflow rates most of the volume of the orifice is filled by this separated region. The necking of the captured flow that occurs near the orifice outlet again constitutes an effective flow area or "vena contracta" of the orifice.

## 3.2 Instrumented Orifice Testing in a Wind Tunnel

To provide further understanding of the details of the interaction shown by the water tunnel tests, a large scale orifice (12.7 mm dia. by 28.6 mm deep) was instrumented with static pressure taps inside the orifice and near the lips in the tunnel side wall. The layout of the taps affording the most insight into the flow field are indicated in Figure 3.

The static pressure taps were monitored with and without flow through the orifice over the range of grazing flow velocity  $26 < V_\infty < 70$  m/sec. The downstream lip pressures confirmed the behavior of the dividing stream surface observed in the water tests. Where there was no flow through the orifice the deflection of the dividing stream surface (see Figure 4a) into and then out of the orifice was manifest by a decrease in the local pressure at the upstream lip and an increase in pressure inside the downstream lip (as high as 12 percent of  $q_\infty$  for  $\delta/D \sim 0.6$ ). As flow is forced out of the orifice, the lifting up of the stream surface is indicated by an increase in the local pressure (above  $P_\infty$ ) at the upstream lip and a decrease in the lip pressures downstream (see Figure 4b). The inverse of this occurs when flow is sucked into the orifice, indicating that the dividing streamline slopes in the opposite direction as indicated in Figure 4(c). These are the salient characteristics of the flow field that were useful in suggesting the analytical model to be presented below. Further details of the flow field obtained from the instrumented orifice tests are discussed in Appendix C.

#### 4.0 THE INVISCID INTERACTION (LID) MODEL

The diagnostic tests showed the behavior of the dividing stream surface between the orifice fluid and the grazing flow passing over the orifice opening. For zero orifice flow the dividing stream surface spans the opening. When there is a slight increase in cavity pressure, fluid is forced out of the orifice by deflecting the dividing stream surface away from the opening at the downstream side while it remains attached upstream. The interaction pressure between the deflected grazing flow and the emerging orifice flow accelerates it downstream parallel to the wall. Thus, the dividing stream surface is like a lid closing off the opening when there is no flow and deflecting upwards as though hinged about the upstream lip when there is outflow (at low flow rates the lid is fairly flat and only acquires significant curvature for high orifice flow rates). Conversely, when there is a slight decrease in cavity pressure (the inflow case), the dividing stream surface (or lid) is again deflected away from the opening, but this time as though hinged about the downstream edge or lip of the orifice. Grazing flow is captured by the lid in this case, and the surface pressure that would be generated in deflecting the captured flow parallel to the lid is assumed to be offset by the reduced pressure in the cavity (to essentially pressure unload the lid). Such simple ideas gleaned from the diagnostic data were used to generate a simplified analytical model to predict the discharge coefficient or resistance of a single orifice in grazing flow.

#### 4.1 Definitions and Assumptions

The fluid which enters or leaves the orifice is assumed to be incompressible. The pressure drop or driving pressure across the orifice is the difference in pressure between the undisturbed grazing flow static pressure and the static (or total) pressure in the cavity, whichever is higher. This pressure drop ( $\Delta P$ ) is related to the ideal orifice flow rate

$$\dot{M}_{id} = \rho A_i V_o \quad (1)$$

where  $A_i$  is the orifice cross-sectional area and  $V_o$  is related to  $\Delta P$  using the incompressible Bernoulli equation

$$\Delta P = 1/2 \rho V_o^2 \quad (2)$$

The effective discharge is defined as the ratio of the actual to the ideal orifice flow rate

$$C_{De} \equiv \dot{M}_{act} / \dot{M}_{id} = \frac{\rho A_o V_o}{\rho A_i V_o} = A_o / A_i \quad (3)$$

where  $A_o$  is the effective flow cross-sectional area (equivalent to the "vena contracta" area used in hydraulics).

The lid model does not involve any assumptions about the behavior of the fluid within the orifice itself and is concerned solely with the opening afforded by the lid for the outflow or inflow of fluid and the pressure forces transmitted across the interface. Thus, no effect of the internal orifice configuration (such as length-diameter ratio) is included and only orifices normal to the wall are considered in this report.

The lid model relationships for both outflow and inflow will be developed for a two-dimensional orifice or slot of infinite aspect ratio assuming inviscid flow (no grazing flow boundary layer). The effect of a boundary layer profile in the grazing flow approaching the orifice is incorporated by substituting area-averaged quantities in the inviscid equations. An adaptation of the two-dimensional analysis to orifices of circular cross-section is shown in Appendix D.

#### 4.2 Lid Model Analysis for Outflow

Figure 5(a) shows the two dimensional model configuration for analysis of the lid model for outflow. The fluid enters the slot at velocity  $V_i$  and is deflected by the interface (or lid) at the orifice outlet through a right angle so that it exits the interaction region at the downstream lip of the slot at velocity  $V_o$  and at the grazing flow pressure  $P_\infty$ .

Continuity for the orifice flow is given by

$$A_i V_i = A_o V_o \quad (4)$$

The effective discharge coefficient is given by

$$C_{De} \equiv A_o/A_i = D \sin \theta / D \approx \theta \quad (\text{for } \theta \ll 1) \quad (5)$$

where  $\theta$  is the deflection of the interface in radians.

The pressure drag on the interface (assumed flat) given by thin aerofoil theory<sup>19</sup> is equated to the momentum of the exiting flow in the downstream direction, using a drag coefficient of  $2\pi\theta$

$$(1/2 \rho V_\infty^2) 2\pi\theta = \rho V_o^2 \quad (6)$$

Combining equations (5) and (6) and eliminating  $\theta$  gives

$$C_{De} = \frac{(V_i/V_\infty)^{2/3}}{\sqrt[3]{\pi}} \quad (7)$$

Thus, a simple power relationship is obtained between discharge coefficient and the ratio of orifice to grazing flow velocity. As will be shown later, experimental data for all orifices tested showed a similar power-law characteristic for the range of orifice velocities of practical interest (i.e.  $V_i/V_\infty < 0.5$ ). The effect of a 1/7 power law turbulent boundary layer profile is incorporated by substituting an average dynamic pressure for the inviscid value in equation (6). The boundary layer dynamic pressure is area-averaged by integrating over the frontal area of the lid. The boundary layer profile is given by

$$V(y) = (y/\delta)^{1/7} V_\infty \quad (8)$$

and the area-averaged dynamic pressure  $q_\infty (\equiv 1/A \int q^A dA)$  is given by

$$\bar{q}_\infty = q_\infty \frac{1}{D\theta} \int_0^{D\theta} (y/\delta)^{2/7} dy \quad (9)$$

which gives

$$\bar{q}_\infty / q_\infty = 7/9 (D\theta/\delta)^{2/7} \quad (10)$$

Upon substituting in equation (6) and eliminating  $\theta$  gives

$$C_{De} = \frac{(9/7)^{7/23} (\delta/D)^{2/23} (V_i/V_\infty)^{14/23}}{0.925} \quad (11)$$

Thus, it is predicted that for outflow the discharge coefficient is proportional to orifice velocity ratio raised to a power slightly greater than one half. By contrast the sensitivity to non-dimensional boundary layer thickness is also a power law but much lower (one seventh the velocity exponent). A good approximation to data obtained by others<sup>14</sup> for slots of 10/1 and 7/1 aspect ratios is

$$C_{De} \sim (V_i/V_\infty)^{0.6} \quad (12)$$

which agrees well with equation (11).

#### 4.3 The Lid Model for Inflow

Figure 5(b) shows the two-dimensional configuration for the analysis of the lid model for inflow. The lid (or dividing stream surface) separates the grazing flow passing the slot from the fluid that is captured by the slot. The captured fluid is deflected by the downstream wall of the slot and exits at velocity  $V_o$  perpendicular to the original grazing flow direction. Writing continuity between the capture area at the upstream lip of the slot and the unseparated flow (or "vena contracta") cross-section entering the cavity gives

$$A_i \theta V_\infty = A_o V_o \quad (13)$$

The effective discharge coefficient defined as before as the exit flow area to the orifice area ratio is obtained from Eqn. (13).

$$C_{De} = A_o/A_i = V_\infty \theta/V_o \quad (14)$$

The next assumptions were suggested by the lip static pressure data which indicated that for low orifice flow rates any change in interface (lid) pressure is negligible compared to the driving pressure or suction in the cavity. Thus, the effect of cavity suction transmitted through the flow field to the pressure side of the lid is to negate or cancel the pressure recovery that would otherwise occur (i.e. were there a lid but no orifice). It is

assumed that the reduced pressure or suction in the cavity accelerates the captured flow parallel to the slot walls to the exit velocity  $V_0$  and that this driving pressure  $\Delta P (= P_\infty - P_c)$  is equal to the pressure on a thin flat placed in the grazing flow at the same angle of attack  $\theta$  as the lid or dividing stream surface. Thus, the dynamic pressure of the fluid exiting the slot is equal to the driving pressure and this is related to the lid angle of attack through thin aerofoil theory. Thus

$$\Delta P = 1/2 \rho V_0^2 = 2 q_\infty \theta \quad (15)$$

Solving for  $\theta$  gives

$$\theta = 1/2 (V_0/V_\infty)^2 \quad (16)$$

Combining equations 13, 14 and 16 and eliminating  $\theta$  gives

$$C_{D_e} = 1/\sqrt{2} (V_i/V_\infty)^{1/2} \quad (17)$$

Thus, again a simple power relationship is obtained between discharge coefficient and the non-dimensional orifice velocity. The exponent and the coefficient for inflow are both slightly less than for outflow, a secondary aspect of the prediction model that repeatedly appears in all the measured data (even for clustered orifices and porous walls).

The effect of a grazing flow boundary layer is incorporated as before by substituting an area-averaged capture velocity in the continuity equation (13) and an area-averaged dynamic pressure in the thin aerofoil pressure equation (15). Again these averages are obtained by integrating from the wall out to the upstream projected height of the lid. The average velocity is given by

$$\bar{V}_\infty/V_\infty = 1/D\theta \int_0^{D\theta} (y/\delta)^{1/7} dy = 7/8 (D\theta/\delta)^{1/7} \quad (18)$$

The average dynamic pressure given by equation (10) and (18) are inserted in equation (15) and (13) respectively which after eliminating  $\theta$  gives

$$C_{D_e} = 0.745 (\delta/D)^{1/16} (V_i/V_\infty)^{7/16} \quad (19)$$

The exponent on velocity ratio for inflow is slightly less than one half and the exponent on boundary layer thickness is again much less (one seventh the velocity ratio exponent). Also the coefficient for inflow is less than that obtained for outflow. All these features of the lid prediction model are shared by the experimental data on single round orifices. The above model analysis required only minor modifications and coefficients as shown in Appendix D to obtain excellent agreement with measured data.

#### 4.4 Concluding Comments on the Lid Model Analysis

Only minor adjustments to the above two dimensional models to account for three dimensional effects were required to obtain agreement with data. The coefficients used in the pressure equations (see Appendix D) are of order unity which suggests the inviscid momentum interaction (Lid) model is an adequate representation of the salient physical factors involved at low orifice flow rates ( $V_i/V_\infty < 0.5$ ). The range over which the model agrees with data extends to large lid deflection angles far beyond the valid range for thin aerofoil theory (for outflow  $\theta_{\max} \approx \pi/8$  and for inflow  $\theta_{\max} \approx \pi/4$ ). So it is clear that at the higher lid deflections the agreement of the model with data is fortuitous and probably due to compensating phenomena not included in the model. More detailed observations of the interaction surface would no doubt improve the form of model but in the meantime what is presented here accounts in reasonably quantitative terms for the major effects of grazing flow velocity ( $V_\infty$ ) and boundary layer thickness to orifice diameter ratio ( $\delta/D$ ). As mentioned above the model does not include any concern with the mechanics of the actual flow within the orifice and hence cannot be used in its present form to make any predictions involving the effects of  $L/D$  of the orifice.

#### 5.0 MEASUREMENTS OF STEADY STATE RESISTANCE OF SQUARE-EDGED ORIFICES IN GRAZING FLOW

It has been shown by Rice<sup>21</sup>, and Budoff and Zorumski<sup>10</sup> and others<sup>22</sup> that grazing flow causes steady state orifice resistance to increase considerably above its non-grazing flow value for low orifice flow rates. This was true for both outflow and inflow though the effects were of different magnitude. For large orifice flow rates (generally beyond the range of interest in engine quieting technology) the resistance again approached the non-grazing flow value.

Measurements of the resistance of several square-edged orifice geometries ( $1\text{mm} \leq D \leq 12.7\text{mm}$ ,  $0.12 \leq L/D \leq 2.0$ ) for a wide range of orifice and grazing flow velocities have been made and will be presented. Data reduction will be discussed followed by a presentation of typical results for one orifice geometry illustrating the general effects of grazing flow on orifice resistance and the ability to collapse resistance data for a wide range of grazing velocities into a single curve whose form was predicted by the inviscid interaction (Lid) model. The predicted effects of grazing flow boundary layer thickness ratio ( $\delta/D$ ) are also compared

with resistance measurements for a wide range of orifice diameters (holding  $\delta$  constant). Orifice length with diameter effects are also presented by comparing data for one hole diameter.

### 5.1 Data Reduction

The pressure drop ( $\Delta P$ ) across the orifice was measured and is given

$$\begin{aligned} \text{for outflow by } \Delta P &= P_c - P_\infty & (20) \\ \text{and for inflow by } \Delta P &= P_\infty - P_c \end{aligned}$$

where  $P_\infty$  is the static pressure of the grazing flow at the orifice station but measured far enough away to be essentially unchanged by the orifice flow, and  $P_c$  is the pressure in the cavity.

Whenever a slight pressure drop was measured for zero orifice flow rate this was subtracted to obtain the pressure drop due to flow. Parenthetically, Franklin and Wallace<sup>20</sup> have shown that even when perfect squareness of the orifice lips and flatness of the duct wall is assured there is still a slight positive cavity pressure measured. In practice for conventionally drilled or punched orifices the zero flow cavity pressure will always differ from the true local grazing flow pressure by a positive or even negative amount (depending on burrs, etc.). For all conditions tested it may be assumed that total and static pressures in the cavity are equal. Flow velocity ( $V_i$ ) through the orifice was obtained by dividing the flow rate measured by rotameter or venturi by the cross-sectional area of the orifice being tested. The one-dimensional incompressible Bernoulli equation is used to obtain the velocity through the "effective vena contracta"  $A_o$  at the orifice outlet pressure ( $P_\infty$  for outflow,  $P_c$  for inflow)

$$\Delta P = 1/2 \rho V_o^2 \quad (21)$$

Then from continuity

$$V_i A_i = V_o A_o \quad (22)$$

and the effective discharge coefficient is given by

$$C_{De} = A_o/A_i = V_i/V_o = V_i/(2\Delta P/\rho)^{1/2} \quad (23)$$

The following identities which follow from eqns. 21, 22 and 23 are useful

$$R \equiv \Delta P/V_i = \Delta P/V_o C_{De} = 1/2\rho \cdot V_i/C_{De}^2 \quad (24)$$

For consistency the density in these equations was taken at grazing flow static conditions ( $P_\infty$ ,  $T_\infty$ ).

## 5.2 Test Results

For each orifice, for the complete grazing flow velocity range tested, discharge coefficient was plotted against the ratio of orifice flow velocity to grazing velocity ( $V_i/V_\infty$ ). As suggested by the lid model for a nearly constant boundary-layer thickness all the data collapsed into two curves, one a correlation of the outflow and the other a correlation of the inflow data. Boundary layer total pressure recovery profiles as shown in Figure (6) were taken in the test section, and confirmed that the boundary layer was turbulent and of approximately constant thickness consistent with a predicted inverse one-fifth power of Reynolds number variation (based on the well known 1/7 power velocity profile).

A typical correlation of the orifice resistance data presented in the equivalent discharge coefficient ( $C_{De}$ ) form is presented in Figure 7. The outflow and inflow correlations of  $C_{De}$  versus orifice velocity ratio ( $V_i/V_\infty$ ) are compared with the non-grazing flow discharge coefficient ( $C_{D0}$ ). In grazing flow the effective discharge coefficient approaches<sup>o</sup> the non-grazing flow value asymptotically for very large orifice flow rates, as might be expected. In contrast, for small orifice flow rates, the effect of grazing flow dominates the orifice discharge coefficient (or resistance) for both inflow and outflow. As resistance is inverse to the square of discharge coefficient (see eqn. 24), it is clear that for low values of velocity ratio ( $V_i/V_\infty$ ) orifice resistance is many times the zero grazing flow value.<sup>i</sup> <sup>8</sup> The differences shown between characteristic shapes of the outflow and inflow data are a key to a better understanding of the large differences between outflow and inflow resistance data noted by Rice<sup>21</sup> and others. Figure 8, constructed by combining Eqn. (24) with the data given in Figure 7, shows resistance as a function of orifice velocity for three grazing velocities 0, 50 and 100 meters/sec. This shows all the characteristics of grazing flow resistance data noted by Rice<sup>21</sup>, and in addition the observation that for very high outflow velocities resistance will drop below the nongrazing flow value. A plausible model to explain this characteristic of the data would be the existence of a reduced mean static pressure around the jet emerging from the orifice analogous to that which can be shown analytically for an ideal fluid flowing around a cylinder. In practice, this regime is generally outside the range of orifice velocities (or equivalent sound pressure levels) of interest in aircraft quieting.

When the discharge coefficient data as shown in Figure 7 is extrapolated towards the origin, the orifice resistance for zero orifice flow rate is indeterminate for both outflow and inflow. An extrapolated resistance plot (Figure 8) of the same data suggests that resistance increased for outflow and decreased for inflow as orifice flow is reduced. A similar trend is apparent in the data of Budoff and Zorumski<sup>10</sup>. To clarify these trends in the data, to obtain typical resistance data over the widest possible range permitted by the instrumentation and in hope of covering the range of equivalent sound pressure levels encountered in jet engines, testing was carried out on one orifice for extremely low orifice flow rates.

### 5.2.1 Resistance Measurements at Low Orifice Flow Rates

Because of the evidence above of a singularity in the data at zero flow, measurements were made of the resistance of an orifice of geometry  $D = 12.7$  mm,  $L/D = 1.0$  to determine if a breakdown in the correlation which is based on an *inviscid* interaction model could be observed. The data obtained is presented in four different ways in Figure 9 through 12. The raw pressure drop versus orifice flow velocity data is shown in Figure 9 showing measurements taken for pressure drops as low as 70 newtons/sq. meter (equivalent to a sound pressure amplitude of 106 db re  $2 \times 10^{-5}$  N/m<sup>2</sup>). Figure 10 shows the correlation of discharge coefficient versus the orifice velocity ratio for all grazing flows tested persisting to the lowest orifice flows for which the pressure drops were measurable using an alcohol manometer at a slant of 5.5 degrees from the horizontal. The low scatter of the data attests to the special care taken to avoid flow pulsations in the grazing flow or the side branch. The same data is displayed in Figure 11 on a log-log scale showing that the power-law form of the correlation suggested by the lid model agrees well with the data down to the lowest flows tested. The singularity which occurs for zero flow for this correlation of the data is displayed as follows. For inflow

$$C_{D_e} = 0.8 (V_i/V_\infty)^{0.47} \quad (25)$$

and the corresponding resistance formula (taking  $\rho = 1.21$  kg/m<sup>3</sup>) is

$$R = 1/2 \rho V_i / C_{D_e}^2 = 0.945 V_i^{0.06} V_\infty^{0.94} \quad (26)$$

Resistance is zero for zero flow rate but the singularity appears in the first derivative with respect to  $V_i$  (i.e., the slope of the resistance curve is singular at zero flow<sup>1</sup> on the inflow side).  
For outflow

$$C_{De} = 0.97(V_i/V_\infty)^{0.534} \quad (27)$$

and resistance is given by

$$R = 0.64(V_i)^{-0.068}(V_\infty)^{1.068} \quad (28)$$

Thus, the correlation for outflow resistance is singular for zero flow. While Budoff and Zorumski's<sup>10</sup> data was the first to suggest similar singular behavior for grazing Mach numbers up to 0.44, more recent data by Feder<sup>22</sup> suggests the same result for grazing flow velocities to 1000 ft./sec. Of course, there are no singularities in real fluid flow and at very low flow rates, approaching zero, viscosity of the flow in the orifice cannot be ignored as in the inviscid interaction (Lid) model. In support of this, the water tunnel tests showed the existence of a (viscous) recirculating region in the orifice neck at vanishingly small orifice through-flow velocities. The minimum orifice Reynolds number for the data shown in Figure 10 is based on diameter. Typical data for a cluster of orifices obtained by Feder<sup>22</sup> is shown in Figure 13 where his resistance data has been replotted in terms of discharge coefficient (based on the face area of the sample rather than the open area). Here the same resistance characteristics for clustered orifices as for a single orifice are shown persisting down to very low orifice velocities (where the minimum Reynolds number based on orifice diameter and the average open area velocity is 45). Thus, for both single orifices and clusters of orifices the effective discharge coefficient for outflow is proportional to  $(V_i/V_\infty)$  raised to a power slightly greater than 1/2 but for inflow the power is slightly less than 1/2. These data tend to support the contention that the flow in or out of a wall orifice is controlled predominantly by the interaction flow field on the grazing flow side of the orifice. Similar data from Feder for a porous facing material is shown in Figure 14.

Note that a first approximation to the data shown in Figure 9 through 12 would be to assume the effective discharge coefficient is proportional to the square root of the velocity ratio  $(V_i/V_\infty)$  and to best fit such a slope to the data as shown in Figure<sup>11</sup>. The correlation so obtained is also shown dotted in Figure 12. This approximation removes the singularity at a cost of deviating from the measurements at very low orifice velocities (or driving pressures - equivalent sound pressures are indicated in Figure 9), under-estimating the resistance for outflow and over-estimating it for inflow.

Inserting the approximation  $C_{D_e} = \alpha(V_i/V_\infty)^{1/2}$  into equation (24) gives for resistance

$$R = (\rho/2\alpha^2)V_i^0 V_\infty^{-1} \quad (29)$$

The effect of this approximation is that orifice resistance becomes independent of orifice velocity  $V_i$  or driving pressure and proportional to grazing flow velocity. Thus, if we assume that steady state and acoustic resistance characteristics are analogous, it may be predicted to a first approximation (1) acoustic resistance in a fixed high speed grazing flow is independent of sound pressure level and (2) acoustic resistance is proportional to grazing flow velocity.

### 5.2.2 Effects of Grazing Flow Boundary Layer Thickness

The lid model prediction that  $C_{D_e}$  is a weak function of boundary layer thickness non-dimensionalized by orifice width or diameter has been tested experimentally by a series of measurements using a wide range of orifice diameters ( $1 \text{ mm} < D < 12.7 \text{ mm}$ ) holding boundary layer thickness and orifice geometry ( $L/D$ ) constant. To make doubly sure of a negligible variation in boundary layer thickness, grazing flow velocity was held within narrow limits ( $35.4 < V_\infty < 39 \text{ m/sec.}$ ).

The data is presented in Figure 15 for a wide range of velocity ratios and a cross-plot for  $V_i/V_\infty = 0.1$  and  $0.2$  is shown in Figure 16 compared to the power law relationship predicted by the lid model. For outflow the agreement with prediction (shown dotted) is excellent. For inflow the increase in discharge coefficient (or decrease in resistance) is greater than predicted when the orifice diameter is less than one quarter of the boundary layer thickness.

It must be pointed out here that the orifice length to diameter ratio ( $L/D = 1.6$ ) for the 1 mm diameter orifice deviates considerably from the nominal value of unity and it may be seen in the next section that this may account for most of the deviation of the data for that orifice from predicted. Nevertheless, it is clear from the data that a power-law exponent close to that suggested by the lid model is a fair approximation to the effect of boundary layer thickness ratio on discharge coefficient over a very wide range

$$\text{i.e.} \quad R \sim (\delta)^{-0.2}$$

Although the exponent for boundary layer thickness is approximately one-fifth that of the grazing flow velocity at the edge of the boundary layer the effect is still significant (e.g. if  $\delta$  doubles then  $R$  decreases by 15 percent) and may not be ignored in duct propagation analysis.

### 5.2.3 Effects of Orifice Length-Diameter Ratio

Correlations of effective discharge coefficient for a series of equal diameter (12.7 mm) square-edged orifices with length to diameter ratios from 0.12 to 2.0 are shown for outflow in Figure 17 and for inflow in Figure 18. These data are summarized in Figure 19.

For outflow the correlation formula

$$C_{D_e} = 0.97(V_i/V_\infty)^{0.5}$$

is a fair approximation to the data for all length-diameter ratios tested. The instrumented orifice tests described in Appendix C showed that the static pressures along the upstream and downstream side-walls of the orifice were not significantly different except just at the lip indicating the orifice is flowing full up to the opening. Then orifice depth would not be expected to affect discharge coefficient and this is here confirmed for the lower velocity ratio range (up to  $V_i/V_\infty = 0.35$ ).

For inflow, the effect of length-diameter ratio is considerable and extends throughout the whole range of orifice to grazing flow ratios tested. (Nevertheless, the exponent of the correlation for all orifices is less than 0.5 as has been observed for all inflow data for single orifices to date). A length-diameter ratio of 0.6 gave the lowest effective discharge coefficient characteristic (i.e., highest resistance) with an increase for lower and higher values.

The increase in effective discharge coefficient for low length-diameter ratios (i.e.,  $L/D < 0.6$ ) has been explained by Stokes et al.<sup>12</sup> as due to the relative ease with which the captured flow enters the cavity as the thickness of the downstream wall of the orifice is reduced. The thinner the wall the less stagnation occurs and the further upstream the cavity depression is felt so more fluid is deflected and captured by the opening.

The increase in discharge coefficient for higher length to diameter ratios ( $L/D > 0.6$ ) is due to pressure recovery within the orifice after the minimum effective flow area or "vena contracta" has been reached. The same mechanism operates for  $L/D > 0.6$  for square-edged orifices in normal flow (see Appendix E).

## 6.0 CONCLUSIONS

(1) The resistance of wall orifices increases in grazing flow due to a momentum interaction mechanism which causes the flow area to be constricted leaving the orifice.

(2) The mechanisms for outflow and inflow, while governed by the grazing flow to orifice flow momentum ratio, operate differently. During outflow the grazing flow blocks the orifice flow at the wall and undergoes deflection to provide the controlling flow area of the orifice. During inflow the captured grazing flow is deflected into the orifice separating at the upstream lip and flowing through a minimum effective area against the downstream wall of the orifice.

(3) An inviscid momentum-drag interaction model based on a simplified configuration of the interface (or lid) between the orifice and grazing flow gave relationships between the major controlling variables which correlated resistance (or effective discharge coefficient) over a wide range of grazing flow velocities, orifice diameters and boundary-layer thickness.

(4) The steady state resistance characteristics for outflow and inflow are different. Therefore the response of a cavity-backed orifice in a grazing flow to sound may not be symmetrical and may involve an adjustment of the mean cavity pressure to equalize the inflow and outflow per cycle.

(5) Resistance data for a wide range of square-edged orifices ( $1.0 \leq D \leq 12.7$  mm,  $0.12 \leq L/D \leq 2.0$ ) correlated for each orifice in the form

$$C_{De} = \alpha(V_i/V_\infty)^n$$

or

$$R = (\rho/2\alpha^2)(V_i)^{1-2n}(V_\infty)^{2n}$$

where  $\alpha$  and  $n$  are correlation coefficients. In general the coefficients  $\alpha$  and  $n$  are different for inflow and outflow (see 4 above).

(e.g. for the following conditions  $D = 12.7$  mm  $L/D = 1.0$   $\delta \approx 9$  mm

$0.004 \leq V_i/V_\infty \leq 0.5$  the following correlations were obtained

$$\text{for outflow } R(\text{Rayl}) = 0.64 V_i^{-0.068} V_\infty^{1.068}$$

$$\text{for inflow } R(\text{Rayl}) = 0.95 V_i^{0.06} V_\infty^{0.94}$$

where velocity is in meters per second.)

(6) A fair approximation to both inflow and outflow data would be a relationship of the form

$$C_{D_e} \sim (V_i/V_\infty)^{1/2}$$

which gives for resistance

$$R \sim (V_i)^0 (V_\infty)^{1.0}$$

suggesting that in high speed grazing flow to first order, acoustic resistance is proportional to  $V_\infty$  and independent of incident sound pressure level.

(7) Increasing grazing flow boundary layer thickness decreases orifice resistance. Resistance is approximately inversely proportional to the one-fifth power of boundary layer thickness to orifice diameter ratio for both inflow and outflow as predicted by the lid model.

(8) The length-diameter ratio of square-edged orifices had a negligible effect on outflow resistance up to a velocity ratio of one-half. For inflow, the length-diameter ratio effect on resistance is significant at all orifice velocities. A maximum resistance (or minimum discharge coefficient) was measured at a length-diameter ratio of six-tenths. Resistance is reduced for thinner orifices probably due to the reduced blockage effect of the downstream wall. It is also reduced for greater orifice depths probably due to pressure recovery after the effective "vena contracta"--as for large L/D orifices in normal flow.

## Appendix A

### Flow Regimes Observed in Water Tunnel

#### Water Tunnel Description

A quasi-two-dimensional open-circuit water tunnel was fabricated from transparent acrylic sheet (plexiglas - 12.7 mm thick). The layout of the tunnel and the valves controlling the main duct and side branch flow rates is shown in Figure 1. The flow within the orifice was made visible by injecting dye (by means of hypodermic syringes through corks) into the cavity or grazing flow as indicated. The maximum grazing flow velocity was limited by the local water supply pressure (and by finger pressure on the plungers of the syringes). The grazing flow cross-section was 25.4 mm x 25.4 mm and the orifice was 12.7 mm wide by 20 mm long x 12.7 mm deep. The cavity was 51 mm diameter. The relative flow rates in the main duct and through the orifice (inflow or outflow) were easily adjusted for steady flow observations. Some limited alternating flow observations were made by squeezing a soft plastic bottle attached to the cavity. Only very low frequency pressure pulses were simulated in this way and no significant differences between steady state and alternating flow regimes were observed.

#### Flow Regimes Description

Depending on the relative level and direction of the orifice flow, five main flow regimes were observed - the zero-net flow, the high or low outflow, and the high or low inflow regimes. The more important features of these regimes are shown schematically in Figure 2.

##### 1. The Zero-Flow Regime (Figure 2a)

When there is no flow through the orifice, the grazing flow induces a recirculating flow within the orifice driven by the shear exerted by the duct fluid passing over the opening. This phenomenon causes the well-known slight inaccuracy of finite-sized wall static pressure taps drilled normal to a surface parallel to the local streamlines. The definitive measurements of Franklin and Wallace<sup>20</sup> showed that a slight positive pressure error results when practical-sized perfectly square-edged wall taps are used. Similar measurements by Shaw<sup>23</sup> and Zogg and Thomann<sup>24</sup> showed further effects of hole configuration and show that the error can be of either sign depending on the hole shape, the presence of burrs, edge radius, etc. Thom and Apelt<sup>25</sup> have demonstrated analytically (for two-dimensional low Reynolds number flow) the existence of the recirculating flow in the hole, the deflection of the dividing streamline into the hole and the increase in local static pressure at the downstream edge. In the water tunnel the recirculation was seen to fill the orifice completely and for the higher duct flow rates the circulating region extended down into the cavity.

##### 2. The Low Outflow Regime (Figure 2b)

When there is a very low net outflow the zone of recirculation

becomes smaller than for zero flow, speeds up on its periphery and is moved over near the downstream lip of the orifice. With further increase in outflow rate the recirculation zone is suppressed altogether. This occurs when the deflection of the grazing flow by the orifice flow is sufficient to lift the dividing surface completely out of the orifice exit plane. The emerging orifice flow is deflected downstream parallel to the wall by pressure and shear forces exerted by the deflected grazing flow on the dividing surface. Thus the grazing flow at first (zero-net flow regime) blocks the orifice opening completely and has its blockage reduced as orifice outflow is increased.

### 3. The High Outflow Regime (Figure 2c)

In this regime the blockage or resistance to flow through the orifice is determined more by inlet conditions (the well-known vena-contracta effect) than by the effects of grazing flow. Penetration into the grazing flow is large and causes separation upstream of the orifice. This regime generally represents pressure amplitudes outside the range of acoustics (e.g. thrust vectoring in rockets, etc.).

### 4. The Low Inflow Regime (Figure 2d)

The net flow drawn into the orifice is low and the zero-net flow circulation becomes a separated region off the upstream lip of the orifice. The separated flow extends through the full depth of the orifice and at first fills up almost the full cross-sectional area of the orifice at entrance to the cavity. As inflow rate increases the cross-section of the separated region at the orifice outlet to the cavity decreases, and thereby the necking or constriction of the orifice inflow. As more grazing flow is captured the dividing surface extending upstream from the downstream edge of the orifice reaches deeper into the grazing flow (boundary layer).

### 5. The High Inflow Regime (Figure 2e)

This regime is characterized by a very steep slope to the dividing surface at the downstream lip indicating that most of the lateral deflection of the orifice flow occurs before entering the orifice. Again (as for the high outflow regime) the direction of flow is predominantly in the direction of the orifice centerline before entering the orifice and resistance is again determined mainly by the vena contracta effect. Neither the high outflow or high inflow regimes are likely to be encountered in jet engine acoustic wall treatments but they represent an interesting limiting cases when the effect of the grazing flow relative to the high orifice flow rate is vanishingly small and orifice resistance approaches the non-grazing flow value.

## Appendix B

### Hersh Acoustical Engineering Wind Tunnel

The Hersh Acoustical Engineering subsonic wind tunnel is a continuous, open, suction type with a rectangular test section 25.4 cm (10 in.) x 12.7 cm (5 in.) and 30.5 cm (12 in.) long. The tunnel has been designed specifically to conduct acoustic testing in a steady uniform grazing flow environment. With the present tunnel drive system, the maximum grazing flow Mach Number is 0.33 (113 m/sec.) but a standby drive system may be installed to give 0.5 Mach Number (170 m/sec.) capability. A schematic of the tunnel as used for steady state testing is shown in Figure B1.

The tunnel drive consisted of a radial blade fan, belt-driven by a 20 H.P. induction motor (1800 RPM synchronous speed). The fan exhausts to atmosphere and the inlet draws air through a stall-free diffuser from the test section and inlet-collector system. The inlet-collector system captures and accelerates ambient air through a rectangular contraction section (16:1 contractor ratio). The capture area is 101.5 cm x 50.7 cm and the walls of the contraction section were contoured so that axial velocity increased monotonically and separation due to overacceleration near the walls was avoided. The contraction section walls were contoured following the guidelines recommended by Rouse and Hassan<sup>26</sup>. The contour consisted of two cubic arcs blended together (i.e. have equal and opposite slopes) at the inflection point. Uniform test section profiles and a 1/7 power turbulent boundary layer profile (i.e. separation-free inlet) have been confirmed for this tunnel over the full velocity range.

The test section made from 12.7 mm (1/2 in.) thick transparent acrylic sheet had one removable side-wall containing the test specimen orifice (or cluster of orifices or perforate). The test specimen was backed by a cylindrical cavity (5 cm - 2 in. dia.) bonded to the sidewall and containing a wall static pressure tap. Flow through the orifice specimen was controlled by means of blowers used in the suction (for inflow) or blowing (for outflow) modes and the side branch or orifice flow rate was metered using either a calibrated Fischer-Porter variable orifice (rotameter) system (range 2.6 - 34,400 cc/minute) or a 12.7 mm (1/2 in.) diameter throat size venturi meter for the highest flow rates.

## Appendix C

### Instrumented Orifice Test Data

A 12.7 mm (1/2 in.) diameter orifice 28.6 mm (1-1/8 in.) deep, was instrumented with static pressure taps inside and near the lip in the tunnel side wall. The layout of the taps (the internal and external lip taps) affording the most insight into the flow field is numbered in the insert in Figure 3. Three cases were considered: (1) zero flow, (2) low outflow, and (3) low inflow.

1. The static pressure taps were monitored first with zero flow through the orifice over the range of grazing flow velocity  $26 < V_{\infty} < 70$  m/sec. The pressures as measured by the pressure taps within the orifice differed negligibly from the cavity pressure ( $P_{\infty}$ ) with the notable exception of the pressure tap labeled  $P_5$  located just inside the downstream lip. Approximately 12 percent of the grazing flow core dynamic pressure ( $q_{\infty}$ ) was recovered here as shown in Figure C1. Notice also the reduced pressure  $P_2$  due to local expansion and the reduced pressure  $P_3$  indicating the existence of a separation bubble near the downstream lip of the orifice. All three pressures are relatable to the local curvature of the dividing stream surface.

2. The variation of internal ( $P_4$  and  $P_5$ ) and external ( $P_2$  and  $P_3$ ) lip static pressures as a function of the ratio of orifice flow velocity to grazing velocity is shown in Figure C2 for the outflow case. The external upstream pressure ( $P_2$ ) is initially slightly negative, as shown in Figure C1 for zero net flow, but becomes increasingly positive for increasing outflow rates because of deceleration of the grazing flow (boundary layer) approaching the orifice. The nearby internal lip pressure ( $P_4$ ) is comparable and represents local deceleration of the flow within the orifice as it stagnates against and deflects the grazing flow passing over the orifice. These pressures increase as the dividing stream surface is deflected further out of the exit plan of the orifice. The downstream internal lip pressure ( $P_5$ ), which is higher than  $P_{\infty}$  as indicated above for zero net flow, decreases as orifice flow increases. It is indicative of the local velocity of the flow inside the orifice or alternately the nearby slope of the dividing-stream surface between the grazing flow and the orifice flow turning the flow parallel to the duct wall. The downstream external lip pressure ( $P_3$ ) becomes increasingly negative indicating the presence of a growing separation bubble as orifice flow increases. In summary, as orifice outflow increases, the dividing stream surface is deflected out from the exit plane of the orifice and the fluid leaving the orifice is deflected and accelerated by drag forces exerted on it by the grazing flow.

3. For inflow, similar static pressure data taken near the orifice lip (upstream and downstream) suggest the manner in which the captured flow is turned and accelerated into the orifice. Figure C3 shows typical data for one grazing velocity ( $V_{\infty}$ ) giving the variation of lip pressures with orifice flow velocity ( $V_1$ ). The pressures outside ( $P_2$ ) and inside ( $P_4$ ) the upstream lip are always less than the undisturbed grazing flow static pressure ( $P_{\infty}$ ) as fluid in this region is simply being accelerated into the orifice under

the influence of the depression in the cavity. The pressure ( $P_5$ ) just inside the downstream lip is higher than  $P_\infty$  for zero flow above as indicated and it increases at first with orifice flow reaching a maximum (recovering 80 percent of the grazing flow dynamic pressure) at an orifice velocity ratio of four-tenths ( $V_1/V_\infty \approx 0.4$ ). As orifice flow is increased still further this pressure continues to decrease as the captured flow tends to be accelerated more and more before it reaches the orifice entrance. The outside downstream lip pressure ( $P_3$ ) which is initially less than  $P_\infty$  for zero orifice flow becomes equal to  $P_\infty$  when  $V_1/V_\infty$  is approximately 0.05 indicating the disappearance of the separation bubble.  $P_3$  is essentially equal to  $P_\infty$  for approximately a five-fold increase in orifice flow indicating the pressure increase due to deflection by the wall downstream of the orifice lip is equal and opposite to the local depression caused upstream when the dividing stream surface is deflected towards the orifice. For higher orifice flows ( $V_1/V_\infty > 0.25$ ) the downstream outside lip pressure  $P_3$  increases with increasing orifice flow.

## Appendix D

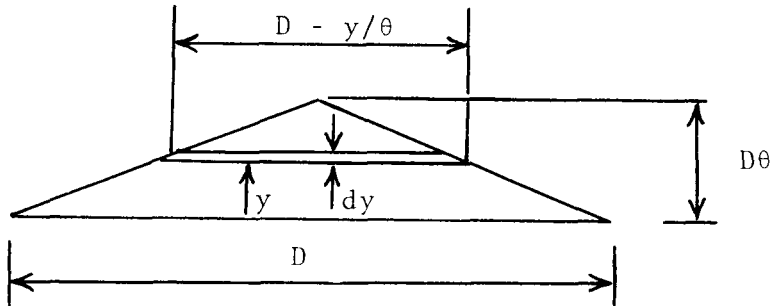
### Extension of Lid Model to Circular Orifices

The two-dimensional inviscid interaction model as derived in Section 4 gives the correct parametric form to the important variables controlling the resistance or discharge coefficient of square edged wall orifices in a grazing flow. Strictly the analysis as given applies only to infinite slots perpendicular to the grazing flow. Although the same form of correlation was obtained for the actual measured data for circular orifices as was predicted for slots, the coefficients and exponents were slightly different. Then it was discovered that a slight modification to the basic input equations which were simple and reasonable to account for the three-dimensionality of the interaction flow field, brought the lid model derivation into almost exact correspondence with the data for circular orifices.

#### For Outflow

Both the continuity and drag relationships were modified in a simple way to account for the three-dimensionality of the orifice outlet and the interaction interface above it. The exit area (or minimum orifice flow area) in the plane normal to the wall at the down-stream lip of the orifice was assumed to be a triangle one orifice diameter wide at the wall surface, and of height  $D\theta$  in the center.

The  $1/7$  power turbulent boundary layer velocity profile is assumed and the effective dynamic pressure acting on the capture triangle is represented as follows



$$\bar{q}_\infty/q_\infty = 2/(D^2\theta) \int_0^{D\theta} (y/\delta)^{2/7} (D - Y/\theta) dy \quad (D1)$$

$$= 49/72 (D\theta/\delta)^{2/7} \quad (D2)$$

The thin aerofoil drag formula (eqn. 6) based on the maximum deflection angle  $\theta$  now clearly overestimates the pressure drag on the interface so the formula was modified by raising  $\theta$  to a power greater than unity and comparing the final equation to experimental data. The slope of the experimental data  $\ln(C_{De})$  Vs  $\ln(V_i/V_\infty)$

agrees fairly well with the final formula obtained analytically when  $\theta$  was raised to the three-halves power. The final result of these modifications was the following relationship for the effective discharge coefficient

$$\begin{aligned} C_{D_e} &= 0.86 (\delta/D)^{4/53} (V_i/V_\infty)^{28/53} \\ &= 0.86 (\delta/D)^{0.0755} (V_i/V_\infty)^{0.529} \end{aligned} \quad (D3)$$

The data for  $D = 12.7$  mm,  $L/D = 0.4$  correlated as

$$C_{D_e} = 0.97 (V_i/V_\infty)^{.537}, (\delta/D = .71) \quad (D4)$$

It is of interest to note that the constant coefficient in (D3) will be brought into correspondence with (D4) if the thin aerofoil formula for drag coefficient is taken as

$$\text{Drag Coefficient} = 1.24 \theta^{3/2} \bar{q}_\infty \quad (D5)$$

#### For Inflow

The cross-section of grazing flow captured by the orifice is assumed to be a symmetrical triangle of base equal to the orifice diameter  $D$  and center height  $D\theta$ . Then continuity between the capture area and the exit area of the orifice is given by

$$A_o V_o = 1/2 D^2 \theta \bar{V}_\infty \quad (D6)$$

where  $\bar{V}_\infty$  is the area-averaged capture velocity for a  $1/7$  power flow turbulent boundary-layer profile given by

$$\begin{aligned} \bar{V}_\infty/V_\infty &= 2/D^2 \theta \int_0^{D\theta} (y/\delta)^{1/7} (D - y/\theta) dy \\ &= 49/60 (D\theta/\delta)^{1/7} \end{aligned} \quad (D7)$$

An expression for the dynamic pressure of the fluid exiting the orifice was assumed to be

$$1/2 \rho V_o^2 = \alpha \bar{q}_\infty \theta^n$$

where  $\bar{q}_\infty$  is the area averaged dynamic pressure of captured grazing flow from equation (D2) and  $\alpha$  and  $n$  are coefficients to be obtained from experimental data. It was found that very good agreement with the experimental measurements was obtained when  $\alpha$  and  $n$  were assumed to be unity giving for the effective discharge coefficient

$$C_{D_e} = 0.84 (\delta/D)^{0.63} (V_i/V_\infty)^{0.437} \quad (D8)$$

The data for  $D = 12.7$  mm  $L/D = 0.4$  correlated as

$$C_{D_e} = 0.8 (V_i/V_\infty)^{0.47}, (\delta/D = .71) \quad (D9)$$

which agrees adequately with prediction (eqn. D8).

## Appendix E

### Discharge Coefficient of Orifices for Non-Grazing Flow

Only data for square-edged orifices is presented in this appendix. A wide range of orifice diameters (1-12.7 mm) and length-to-diameter ratios ( $0.12 < L/D < 3.14$ ) were tested. The orifices were drilled in plexiglas sheet taking care to avoid any cracking or chipping of the holes at entry or exit. The flow rate through the orifice and the pressure drop across it were measured over a wide range. The variable area flowmeter readings were corrected for ambient temperature, and the volume flow rate was divided by the orifice cross-sectional area to give the orifice entrance velocity ( $V_e$ ). The total pressure drop across the orifice was taken as the difference in static pressure between the cavity and ambient pressure. Negligible error is involved in assuming cavity static and total pressure to be equal.

The discharge coefficient of a wide range of orifice diameters and length/diameter ratios was measured. For the Reynolds number range where  $C_{D0}$  is insensitive to flow through the orifice (i.e., Reynolds number based on inlet velocity and diameter,  $Re = V_e D/\nu$ ) no significant effect of diameter was observed ( $1 \text{ mm} < D < 12.7$ ). On the other hand,  $C_{D0}$  is shown to be very sensitive to length/diameter particularly in the range  $0.4 < L/D < 1.0$  as illustrated in Figure E1. It may be noted, in passing, that  $C_{D0}$  is also affected by other geometrical factors such as existence of burrs, radiusing of the entrance, etc. In these tests such effects were carefully avoided.

The effect of lowering Reynolds number (based on inlet velocity and diameter) below the Bernouilli regime is shown in Figure E2 for the smallest orifice tested ( $D = 1$  millimeter). It can be seen that  $C_{D0}$  decreases when Reynolds number is less than approximately  $10^3$ . Steady-state orifice resistance will then be no longer proportional to velocity but will have a higher value inversely proportional to the square of the actual discharge coefficient.

## LIST OF SYMBOLS

$A_i$	orifice or slot cross-sectional area, square meters ( $m^2$ )
$A_o$	minimum flow area of orifice flow, square meters ( $m^2$ )
$c$	speed of sound, meters per second (m/sec)
$C_{De}$	effective discharge coefficient with grazing flow
$C_{Do}$	discharge coefficient with zero grazing flow
$D$	diameter of circular orifice or width of two-dimensional slot, meters (m)
$L$	orifice depth, meters (m)
$\dot{M}_{act}$	actual orifice mass flow rate
$\dot{M}_{id}$	ideal orifice mass flow rate
$n$	an exponent
$P_1, P_2, P_3, P_4, P_5$	orifice lip wall static pressure, Newtons per square meter ( $N/m^2$ )
$P_c$	pressure in cavity, Newtons per square meter ( $N/m^2$ )
$P_{T_\infty}$	grazing flow total pressure, Newtons per square meter ( $N/m^2$ )
$q_\infty$	grazing flow dynamic pressure, Newtons per square meter ( $N/m^2$ )
$R$	orifice resistance $R \equiv \Delta P/V_i$ , Rayls ( $Kg/m^2 \cdot sec$ )
$V_i$	orifice flow velocity based on cross-sectional area $A_i$ , meters per second (m/sec)
$V_o$	orifice one dimensional flow velocity based on minimum flow area $A_o$ , meters per second (m/sec)
$V_\infty$	grazing flow velocity (not in boundary layer), meters per second (m/sec)
$y$	distance from wall, meters (m)
$\alpha$	coefficient
$\delta$	boundary layer thickness, meters (m)
$\Delta P$	denotes differential pressure
$\theta$	angle of attack or deflection in radians
$\rho$	density in kilograms per cubic meter ( $Kg/m^3$ )

## References

1. Morse, P.M., "The Transmission of Sound Inside Pipes", J. Acoust. Soc. Am., Vol. 11, 1939, p. 205.
2. Cremer, L. Akust. Beih. 2,249-263, 1953, (translated by G.B. de Montolvo of McDonnell Douglas Aircraft Co.).
3. Rice, E.J., "Propagation of Waves in an Acoustically Lined Duct with a Mean Flow", NASA SP-207, 345-355, Basic Aerodynamic Research Conference, 1969.
4. Zorumski, W.E. and Parrott, Tony L. "Nonlinear Acoustic Theory for Rigid Porous Materials", NASA TND-6196, June 1971.
5. Hersh, A.S. and Rogers, T., "Fluid Mechanical Model of the Acoustical Behavior of Small Orifices", Paper No. 75-495, AIAA 2nd Aero-Acoustics Conference, March 1975.
6. Groeneweg, John F., "Current Understanding of Helmholtz Resonator Arrays as Duct Boundary Conditions", NASA SP-207, pp. 357-368, Basic Aerodynamic Research Conference (1969).
7. Plumblee, Harry E/ Jr., Dean, Peter D., Wynne, George A., and Burrin, Robert H., "Sound Propagation in and Radiation from Acoustically Lined Flow Ducts; A Comparison of Experiment and Theory", NASA CR-2306, Oct. 1973.
8. Feder, E., and Dean III, L.W., "Analytical and Experimental Studies for Predicting Noise Attenuation in Acoustically Treated Ducts for Turbofan Engines", NASA CR-1373, Sept. 1969.
9. Armstrong, D.L., "Acoustic Grazing Flow Impedance using Waveguide Principles", NASA CR-120848 (Dec. 12, 1971).
10. Budoff, Marvin and Zorumski, William E., "Flow Resistance of Perforated Plates in Tangential Flow", NASA TM X-2361, Oct. 1971.
11. Dittrich, R.T. and Graves, C.C., "Discharge Coefficients for Combustor-Liner Air-Entry Holes, I-Circular Holes with Parallel Flow", NACA TN-3663, April 1956.
12. Stokes, G.M., Davis, Jr. D.D., and Sellers, T.B., "An Experimental Study of Porosity Characteristics of Perforated Materials in Normal and Parallel Flow", NACA TN-3085, 1954 (Supersedes NACA RM L53H07).
13. Haukohl, J., Forkois, J.L., and Roberson, S.J., "Orifice In-Flow Efficiency Tests", Vol. I, "Test Results"; Vol. II, "Application to Shuttle Venting During Reentry", NASA CR-61383, March 1972.
14. Walters, W.P., Glasgow, R.M., and Baker, J.M., "Generalized Gaseous Discharge Characteristics of Flat Plate Orifices", Nortronics-Huntsville, Huntsville, Ala., TR-794-8-434, Nov. 1968.

15. Goethert, H., "Transonic Wind Tunnel Testing", AGARD Pergamon Press, 1961.
16. Ingard, Uno, "Absorption Characteristics of Nonlinear Acoustic Resonators", J. Acoust. Soc. Am. Vol. 44, pp. 1155-1156, 1968.
17. Rice, E.J., "A Model for the Pressure Excitation Spectrum and Acoustic Impedance of Sound Absorbers in the Presence of Grazing Flow", AIAA Paper No. 73-995, Aero-Acoustics Conference, Seattle, Wash., Oct. 1973.
18. Sirignano, W.A., and Tonon, T.S., "Nonlinear Aspects of Combustion Instability in Liquid Rocket Motors", NASA CR-72426, June 1968.
19. Kuethe, A.M., and Schetzer, J.D., "Foundations of Aerodynamics", Chapter 5, John Wiley and Sons, 1950.
20. Franklin, R.E., and Wallace, James M., "Absolute Measurements of Static-Hole Error Using Flush Transducers", J. Fluid Mech. (1970), Vol. 42, Part 1, pp. 33-48.
21. Rice, Edward J., "A Model for the Acoustic Impedance of a Perforated Plate Liner with Multiple Frequency Excitation", NASA TM-67950, 1971.
22. Feder, Ernest, "Effect of Grazing Flow Velocity on the Steady Flow Resistance of Duct Liners", Pratt and Whitney Aircraft Report, No. 5051, July 8, 1974.
23. Shaw, R., "The Influence of Hole Dimensions on Static Pressure Measurements", J. Fluid Mech. (1960), Vol. 7, pp. 550-564.
24. Zogg, H., and Thomann, H., "Errors in Static Pressure Measurements Due to Protruding Pressure Taps", J. Fluid Mech. (1972), Vol. 54, Part 3, pp. 489-494.
25. Thom, A., and Apelt, C.J., "The Pressure in a Two Dimensional Static Hole at Low Reynolds Numbers", 1957, Aero, Res. Council. R & M 3090.
26. Rouse, H., and Hassan, M.W., "Cavitation-free Inlets and Contractions", Mechanical Engineering, March 1949, pp 213-216.

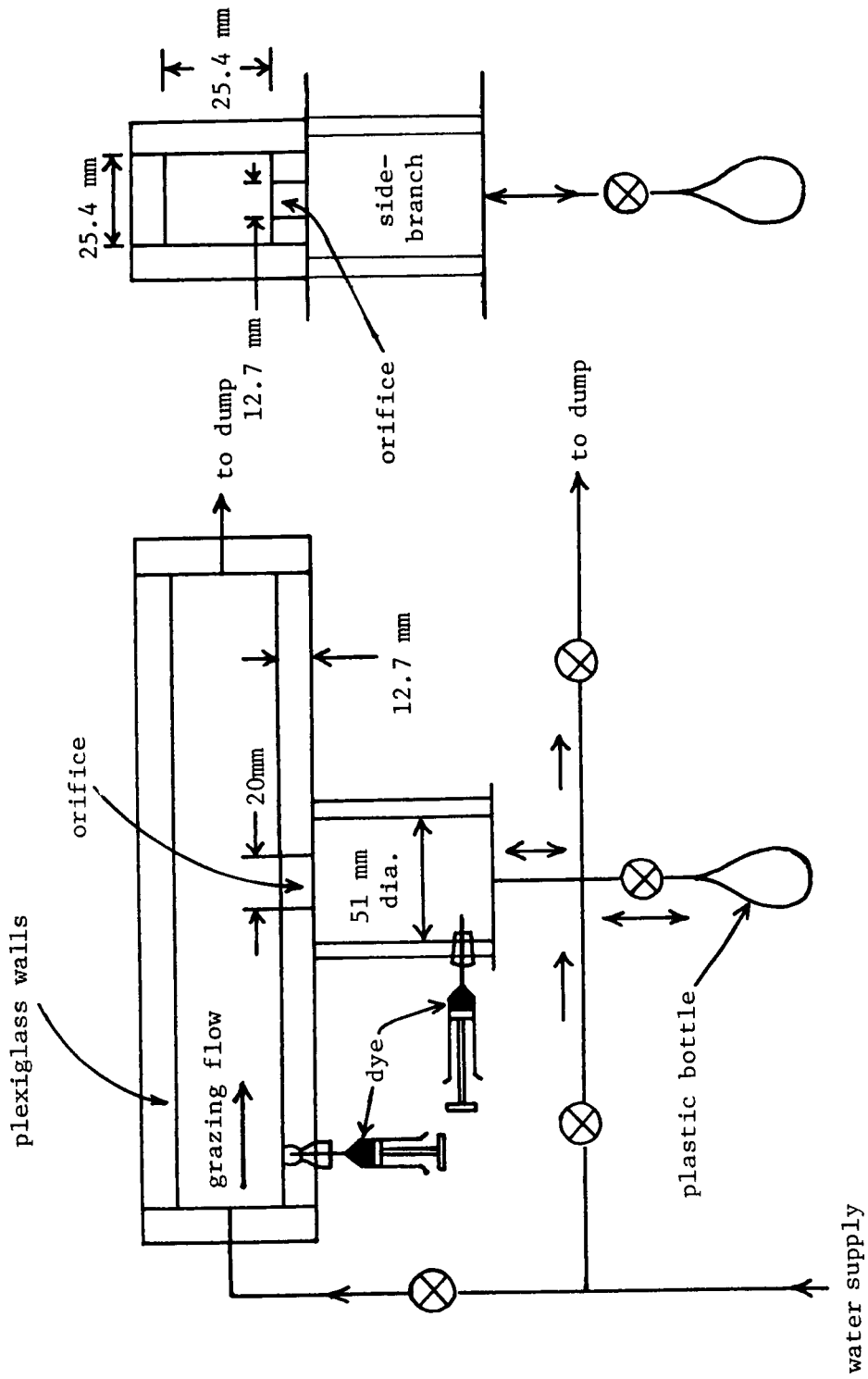


FIGURE 1. SCHEMATIC OF WATER TUNNEL

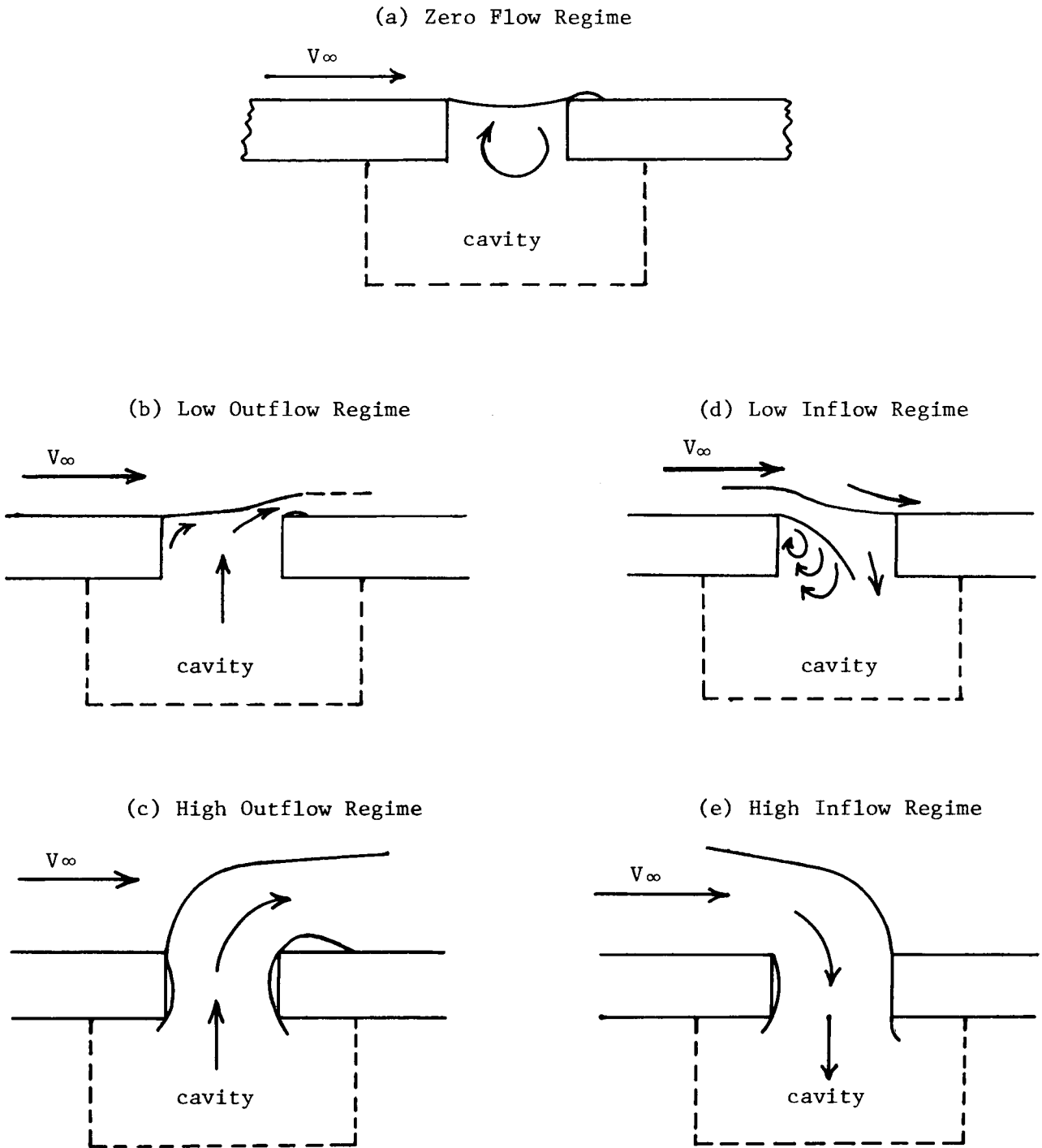


FIGURE 2. FLOW REGIMES OBSERVED IN WATER TUNNEL

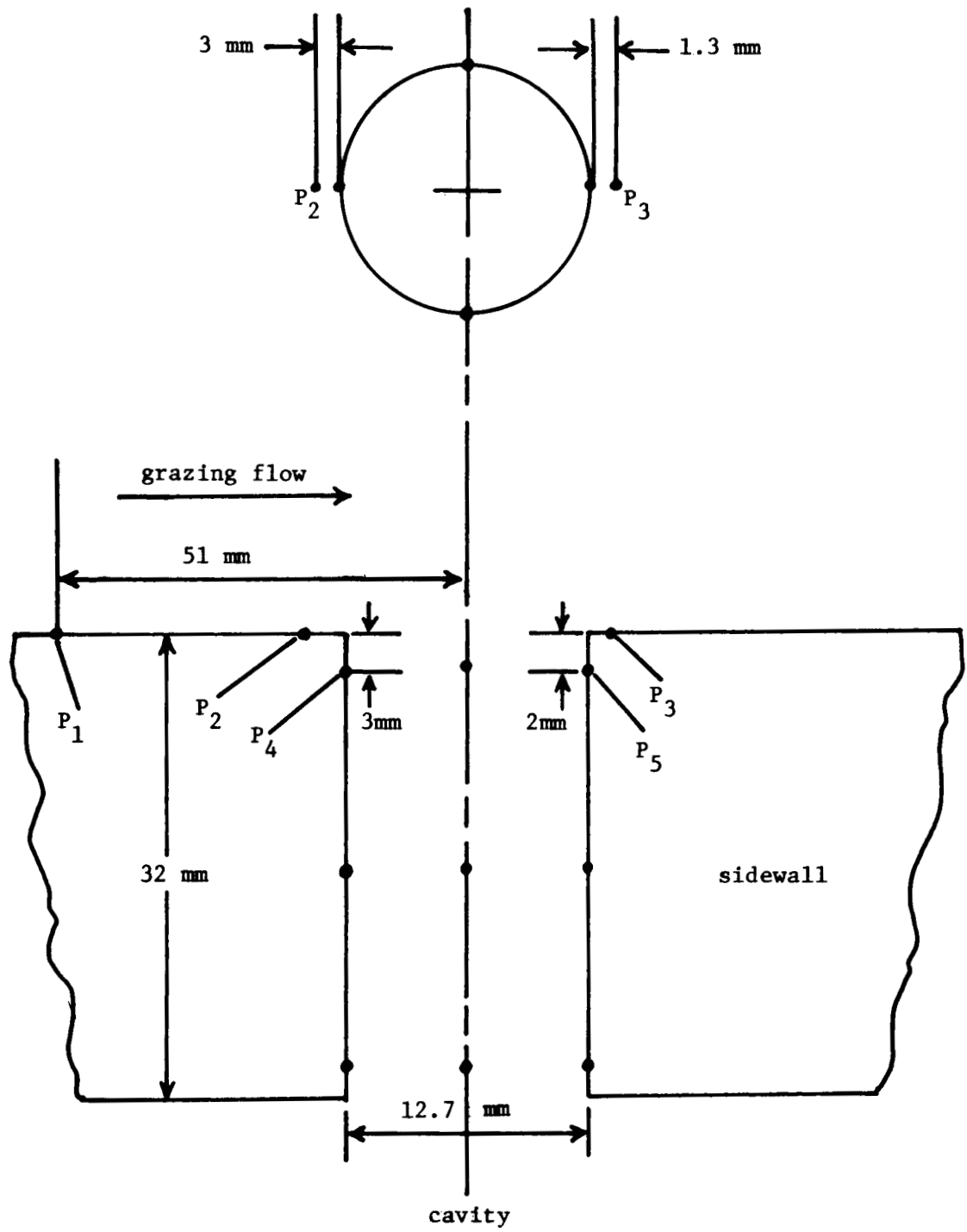


FIGURE 3. LAYOUT OF STATIC TAPS IN INSTRUMENTED ORIFICE

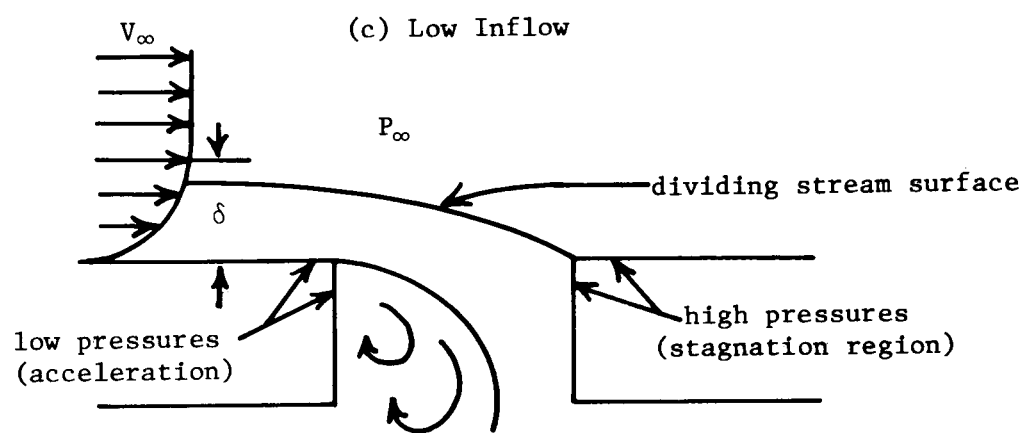
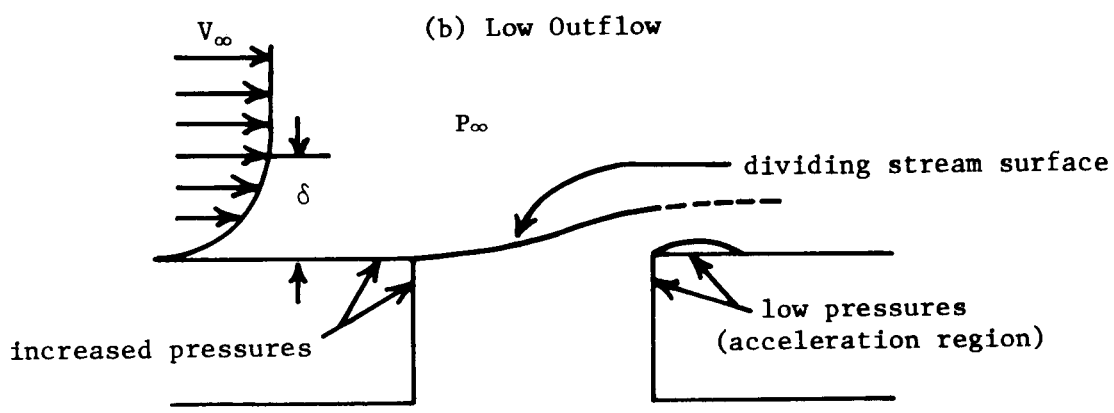
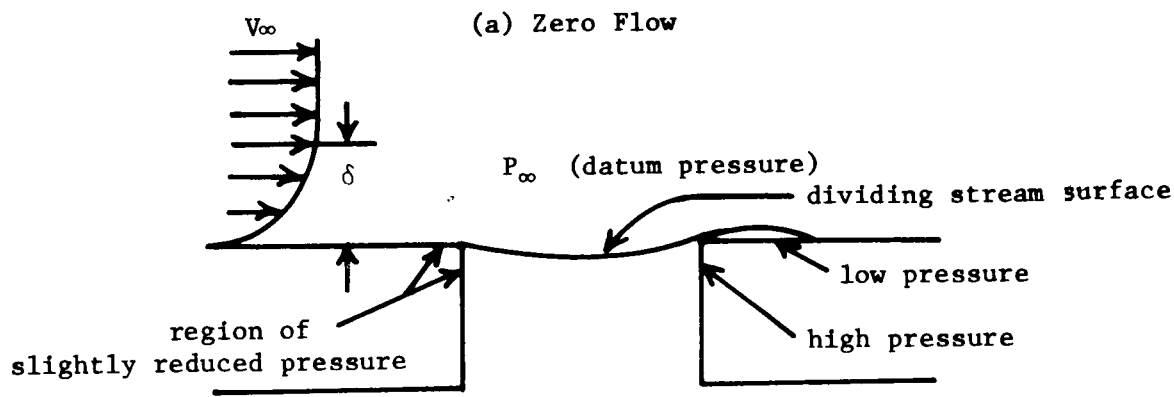
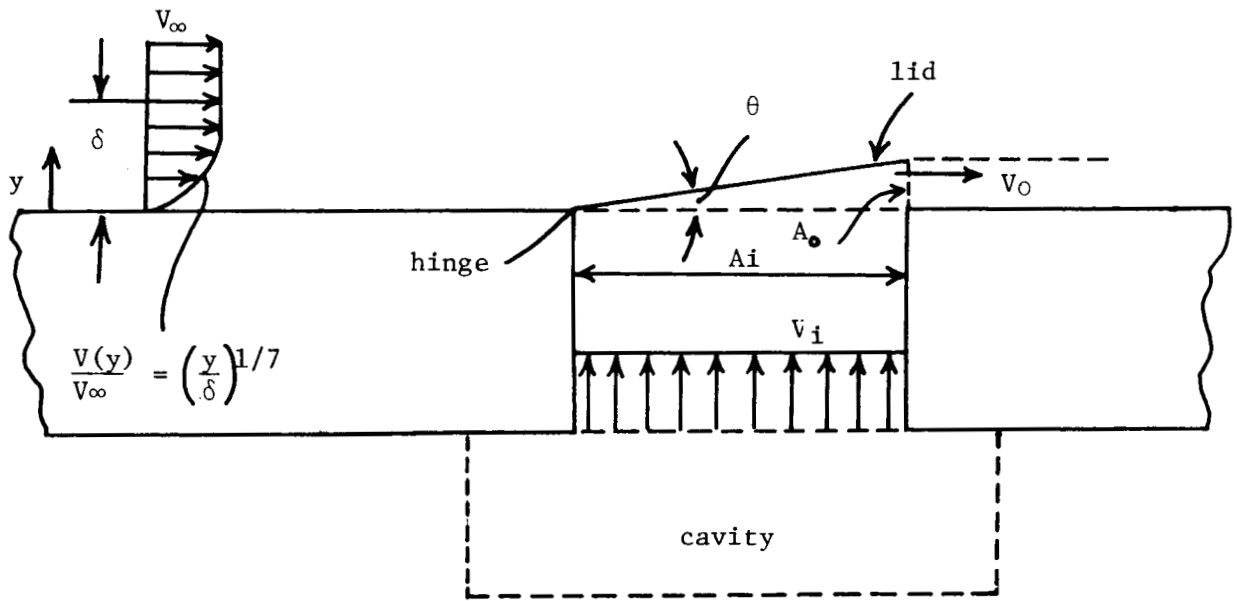
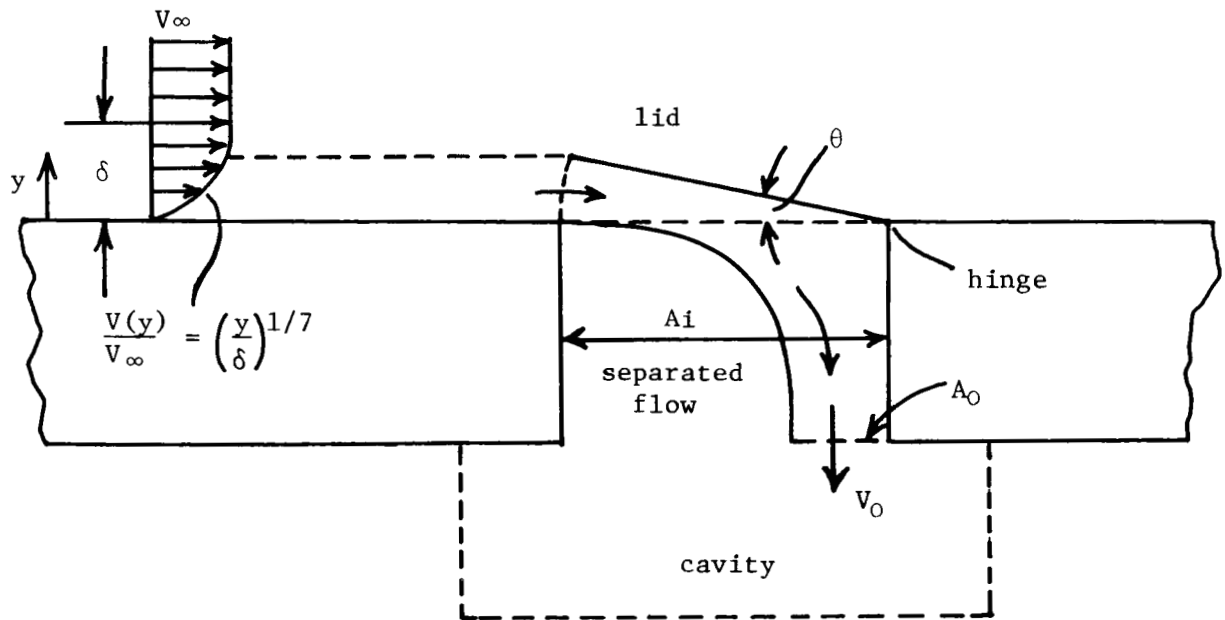


FIGURE 4. DIVIDING STREAM SURFACE CHARACTERISTICS OBTAINED FROM DIAGNOSTIC TESTING



(a) Schematic of Lid Model for Outflow



(b) Schematic of Lid Model for Inflow

FIGURE 5. THE LID MODEL

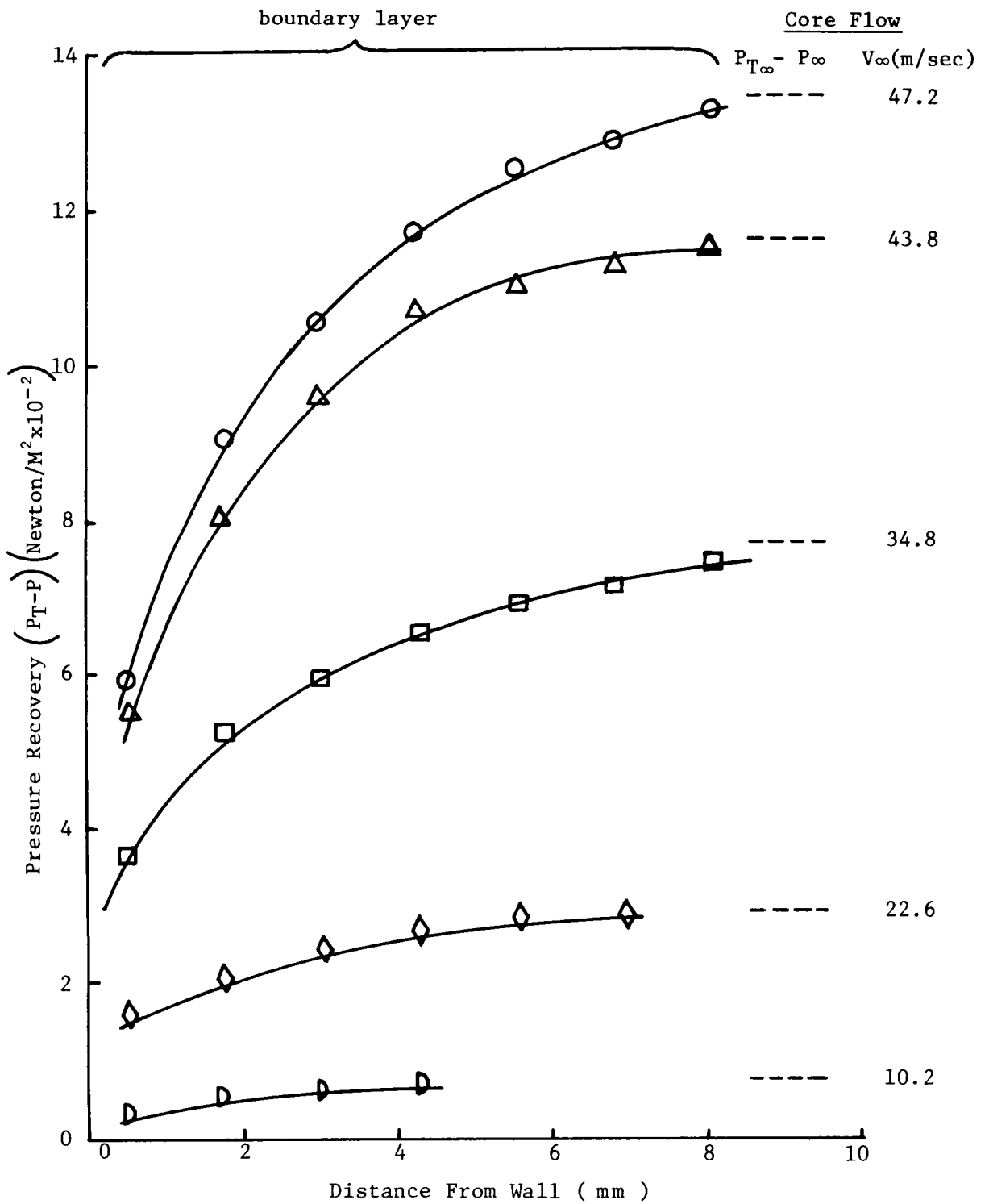


FIGURE 6. BOUNDARY LAYER PROFILES IN TEST SECTION

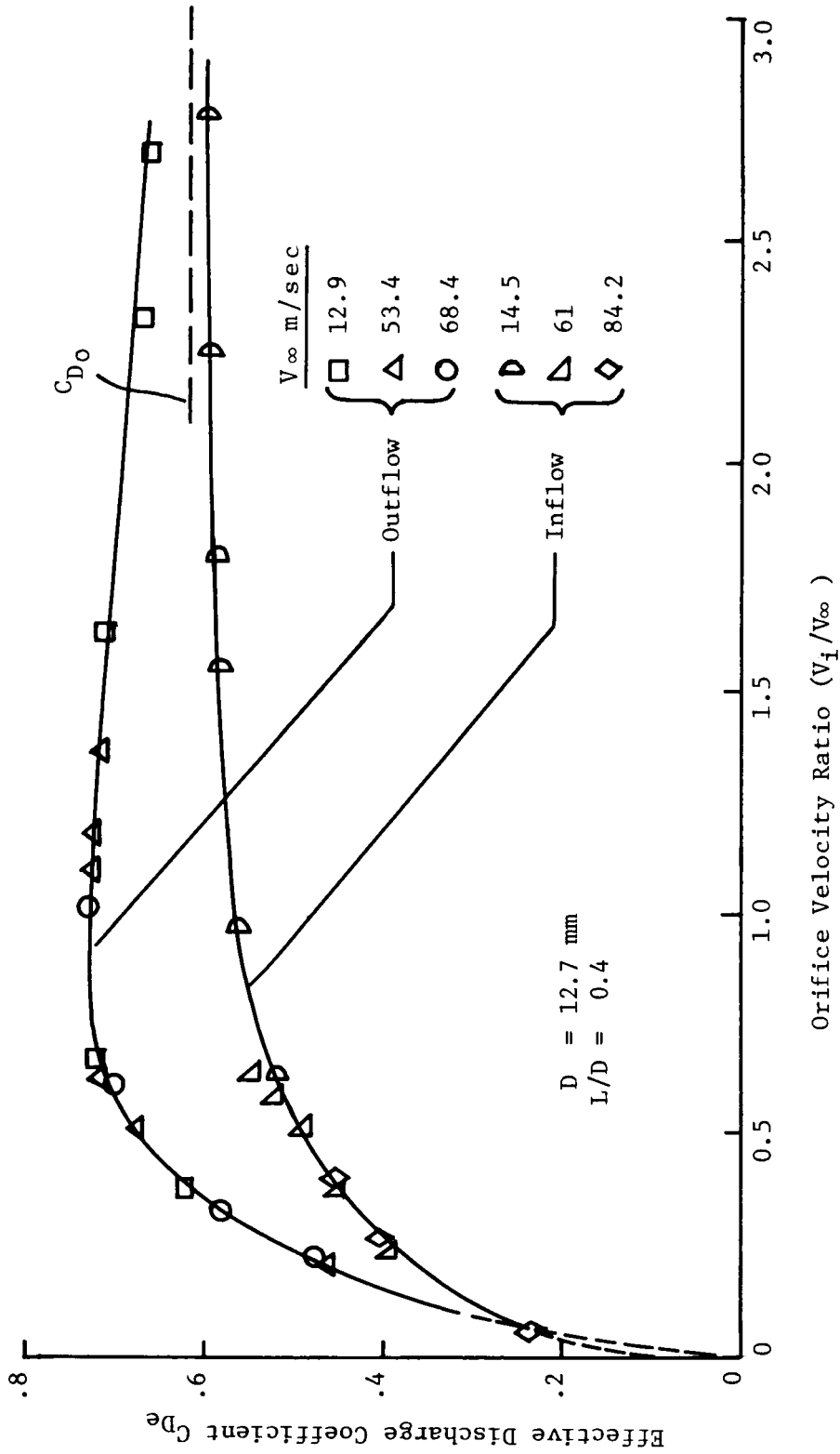


FIGURE 7. TYPICAL CORRELATION OF GRAZING FLOW DATA

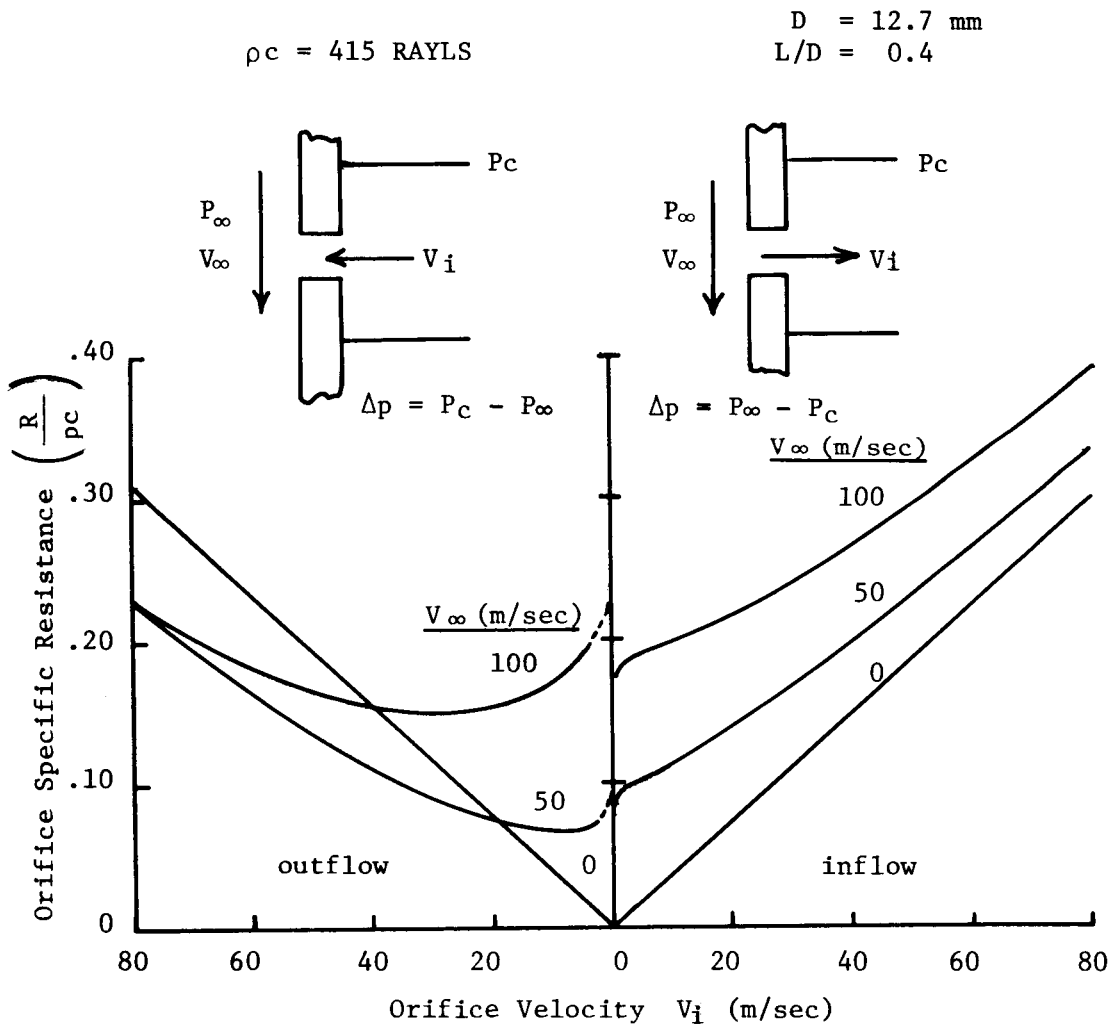


FIGURE 8. TYPICAL EFFECT OF GRAZING FLOW ON ORIFICE RESISTANCE

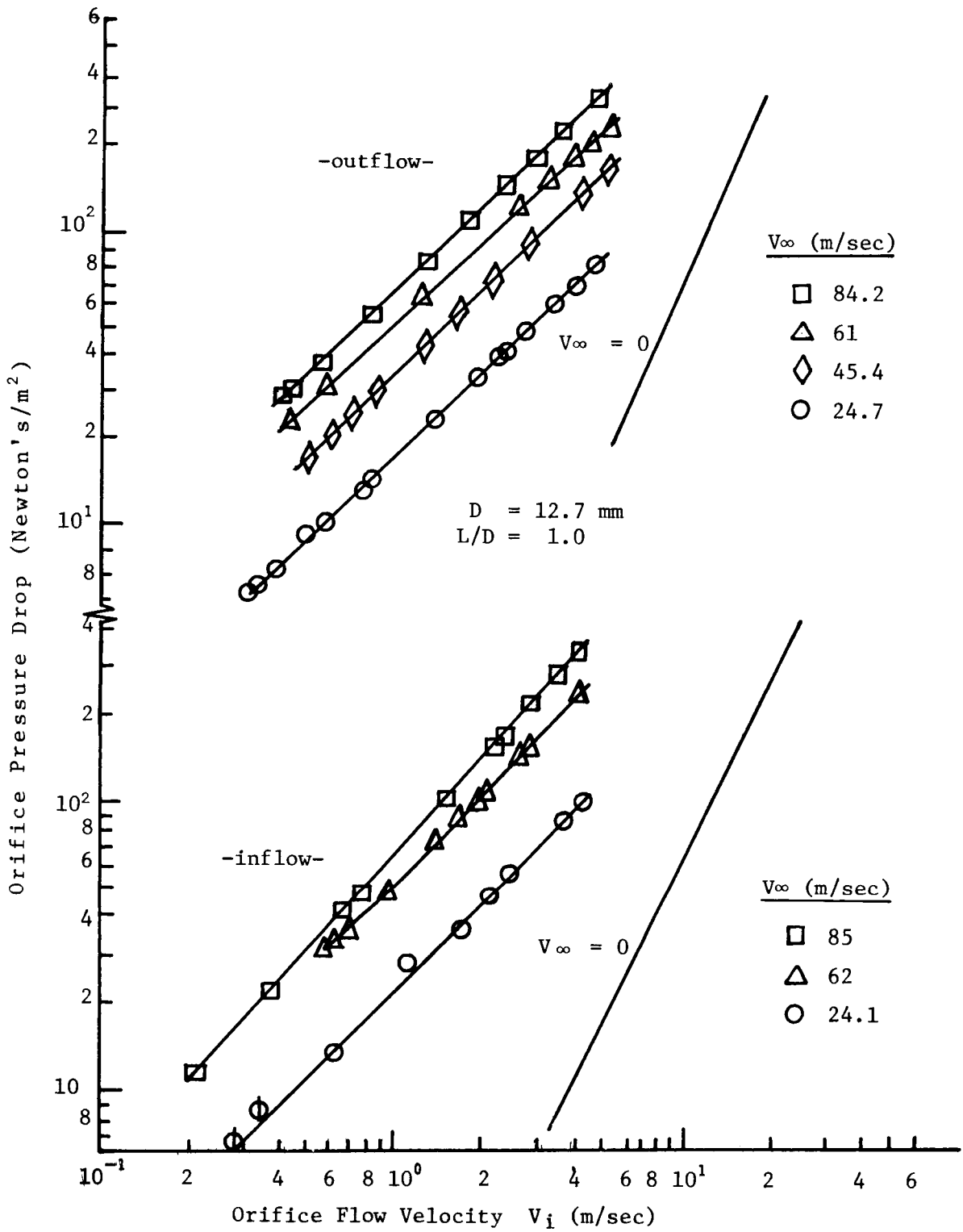


FIGURE 9. TYPICAL PRESSURE DROP VS VELOCITY DATA

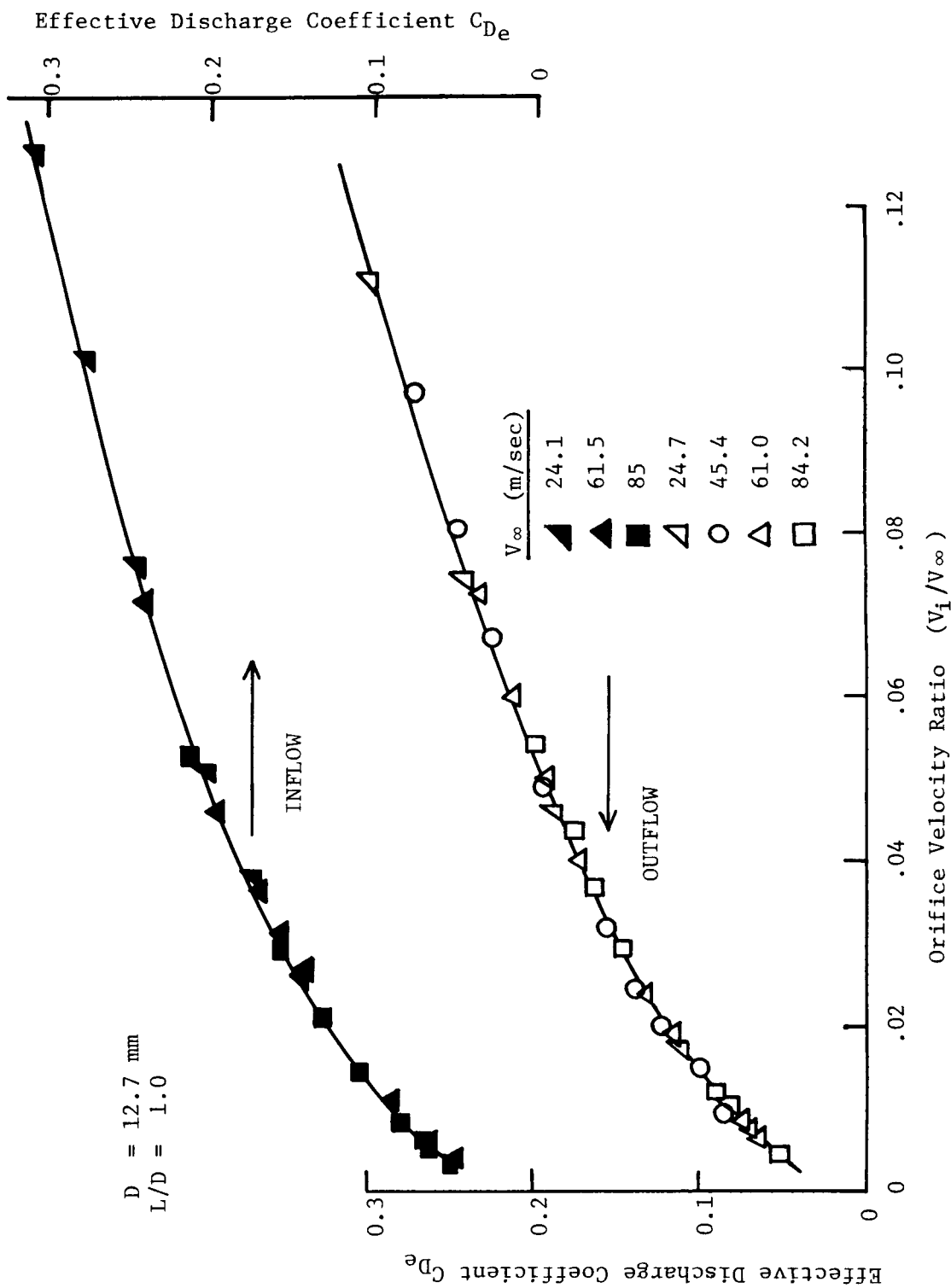


FIGURE 10. TYPICAL CORRELATION OF EFFECTIVE DISCHARGE COEFFICIENT  $C_{DE}$  FOR LOW FLOW RATES

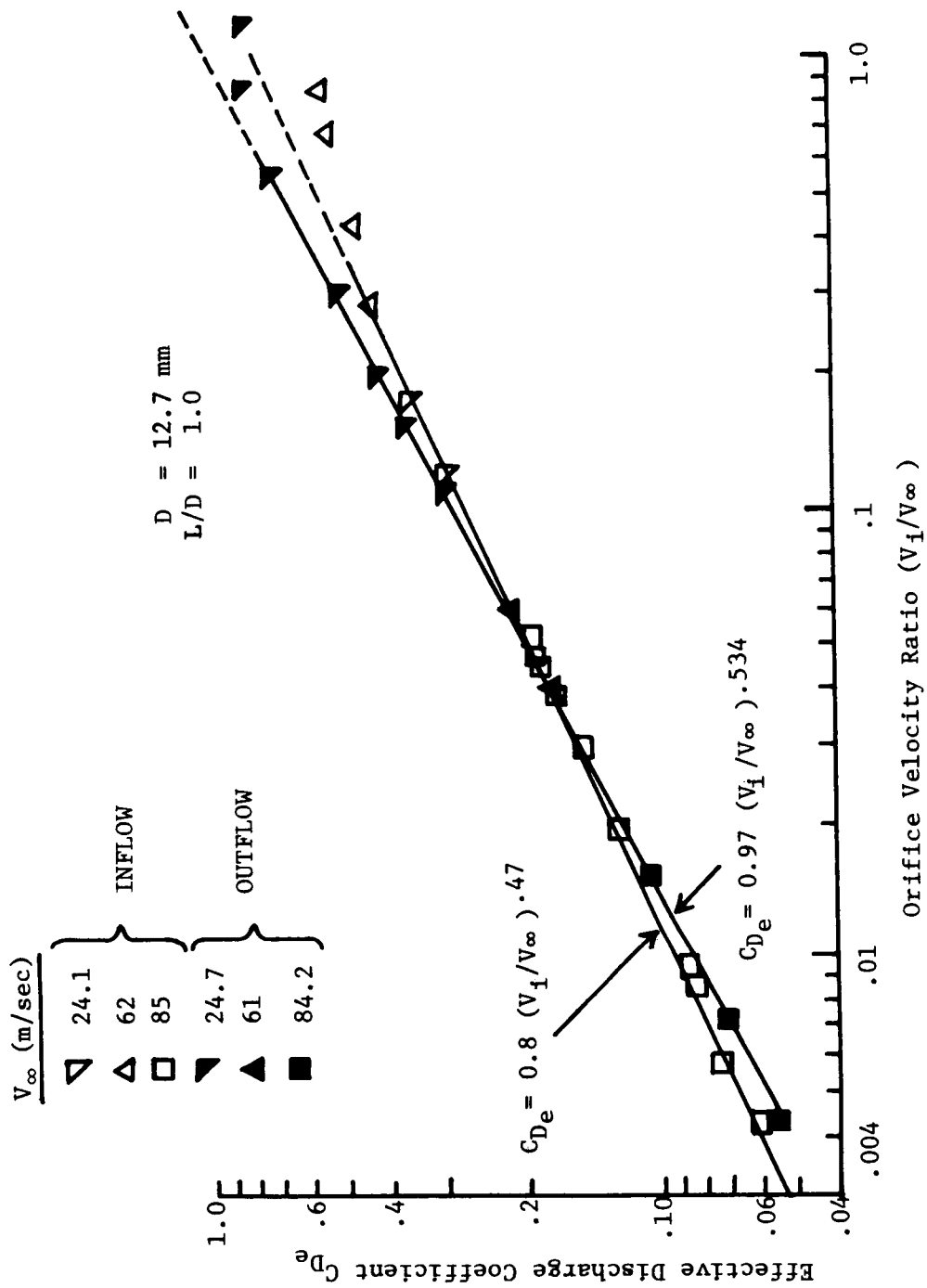


FIGURE 11. TYPICAL LOW ORIFICE FLOW RESISTANCE DATA

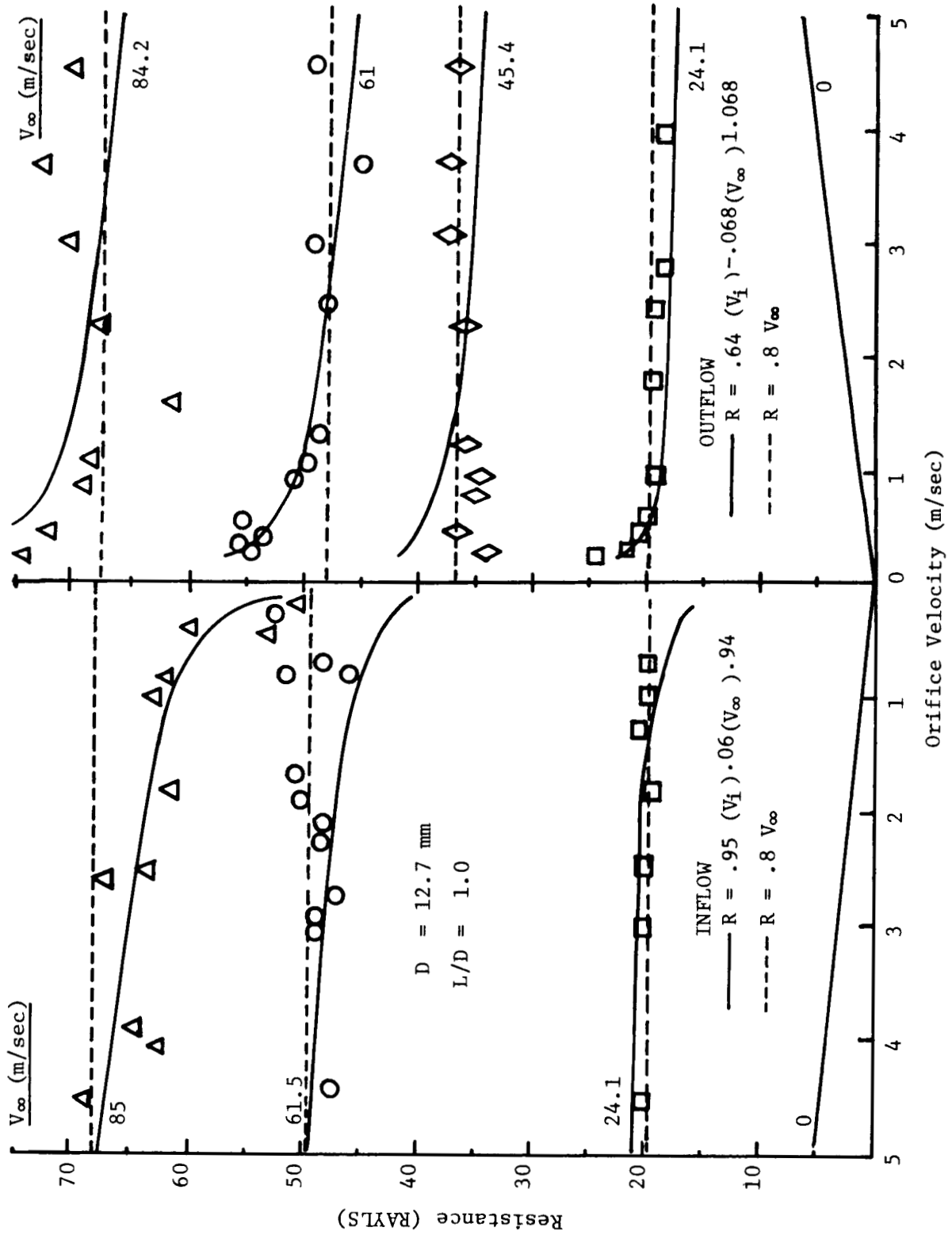


FIGURE 12. TYPICAL LOW ORIFICE FLOW RESISTANCE DATA

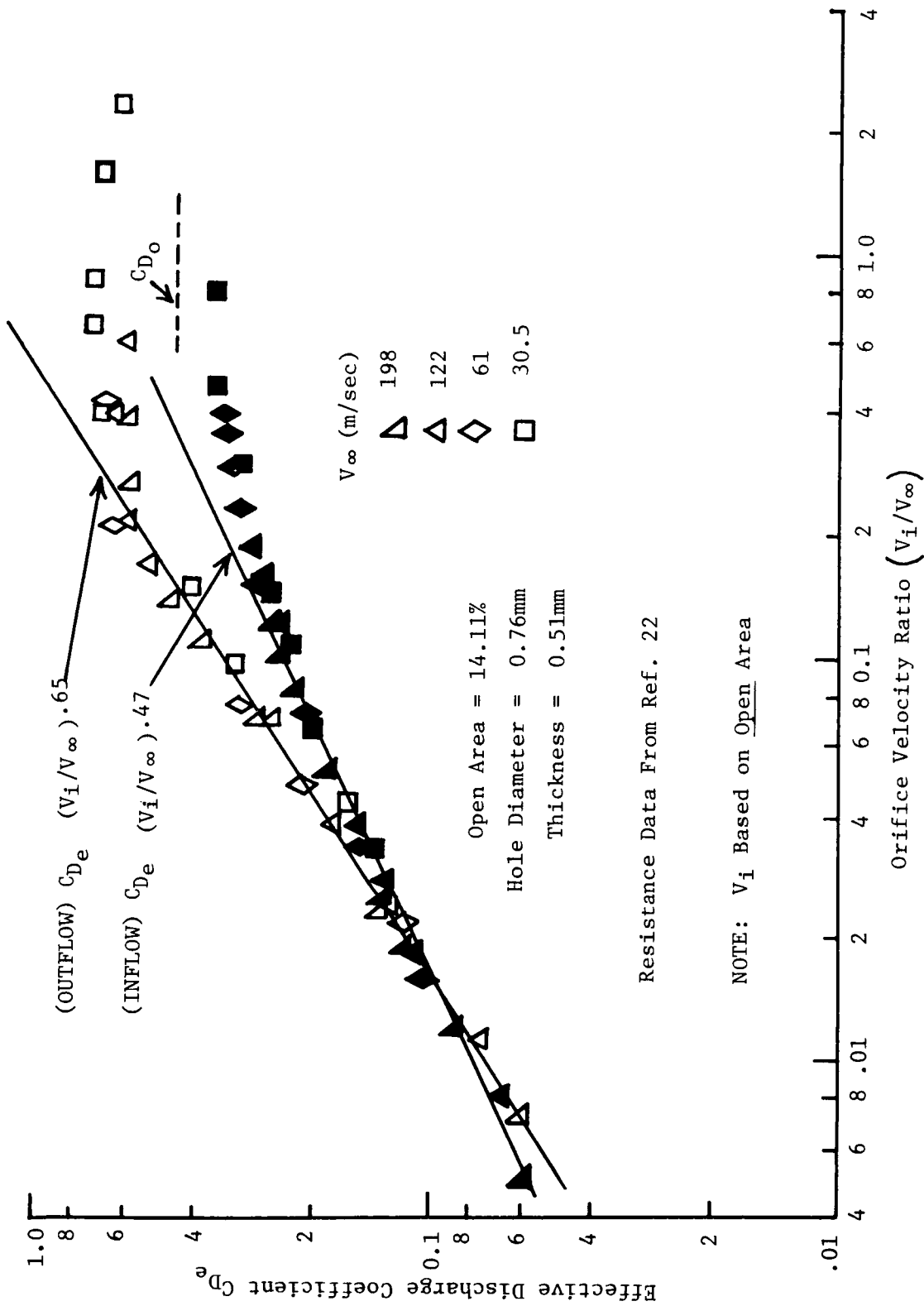


FIGURE 13. TYPICAL CORRELATION OF DATA FOR CLUSTERED ORIFICES

Raw Data From Ref. 22

Material - 4 RAYL POLYIMIDE

Symbols

Open - OUTFLOW

Solid - INFLOW

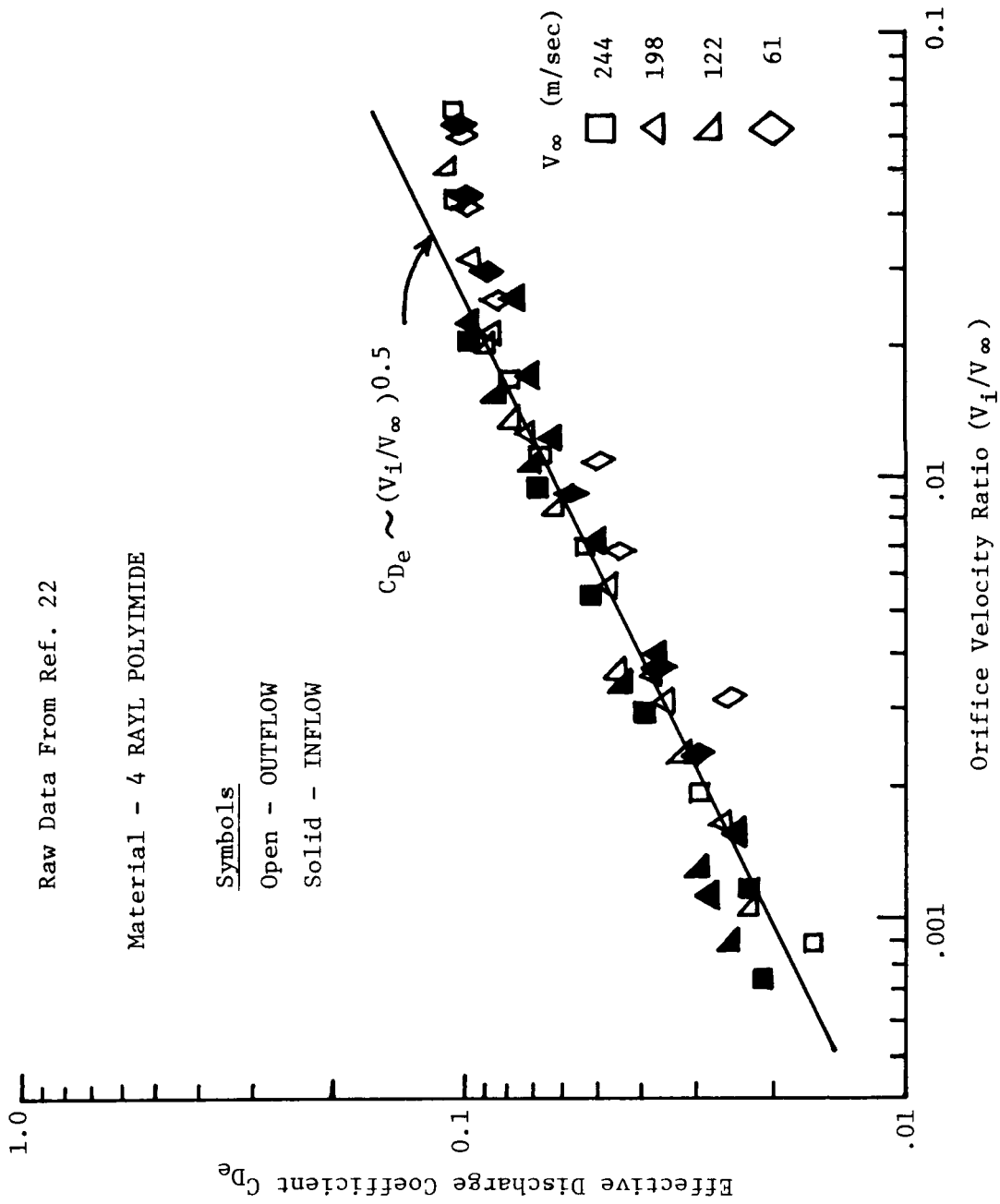
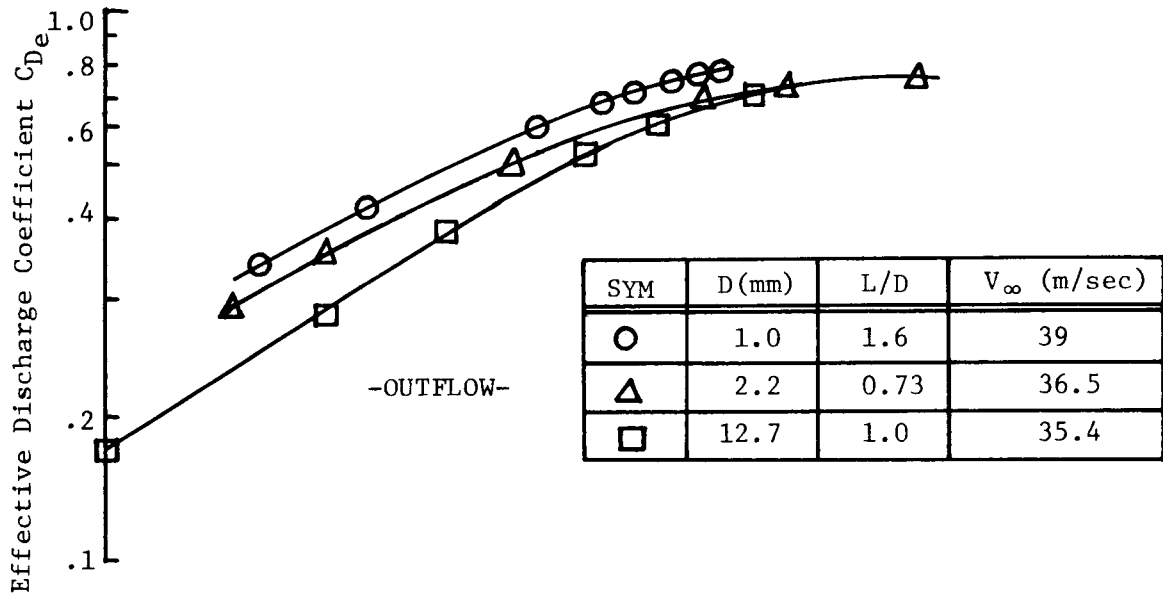


FIGURE 14. CORRELATION OF DATA FOR POROUS FACING MATERIAL



Boundary Layer Thickness ( $\delta$ )  $\approx$  9 mm

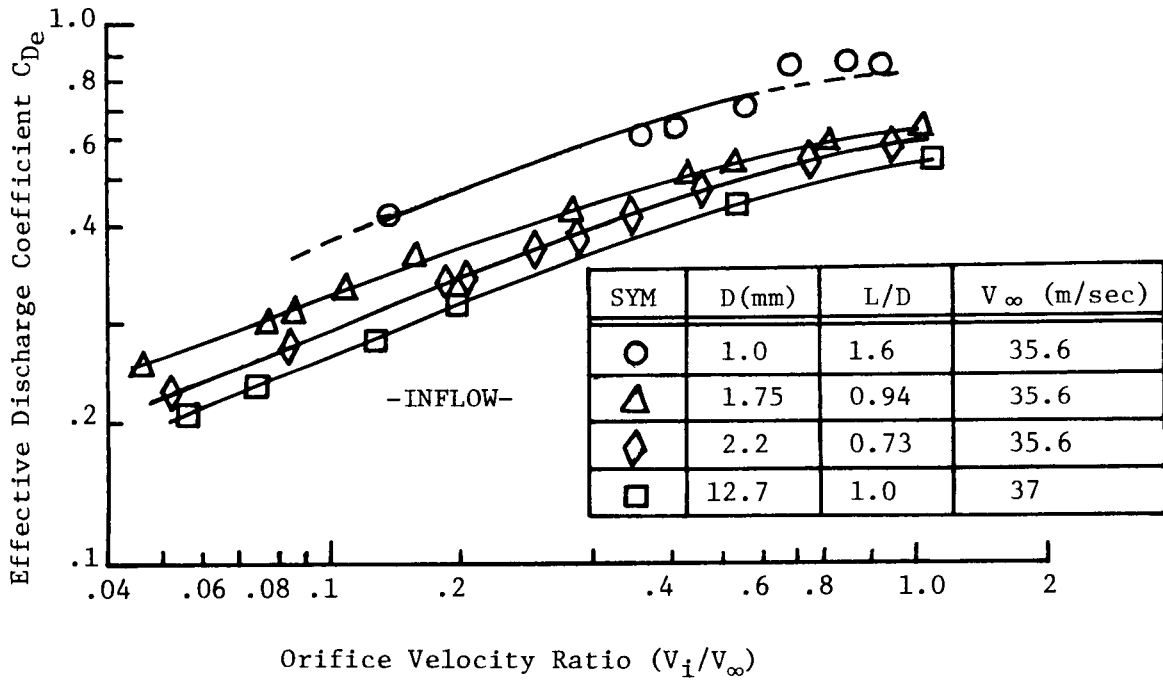


FIGURE 15. EFFECT OF BOUNDARY LAYER THICKNESS RATIO ( $\delta/d$ ) ON EFFECTIVE DISCHARGE COEFFICIENT ( $C_{De}$ )

SYM	Dmm	L/D	$V_\infty$ m/sec
○	1	1.6	35.6
△	1.75	0.94	35.6
◇	2.2	0.73	35.6
□	12.7	1.0	37

$V_\infty = 37$  m/sec

$\delta \approx 9$  mm

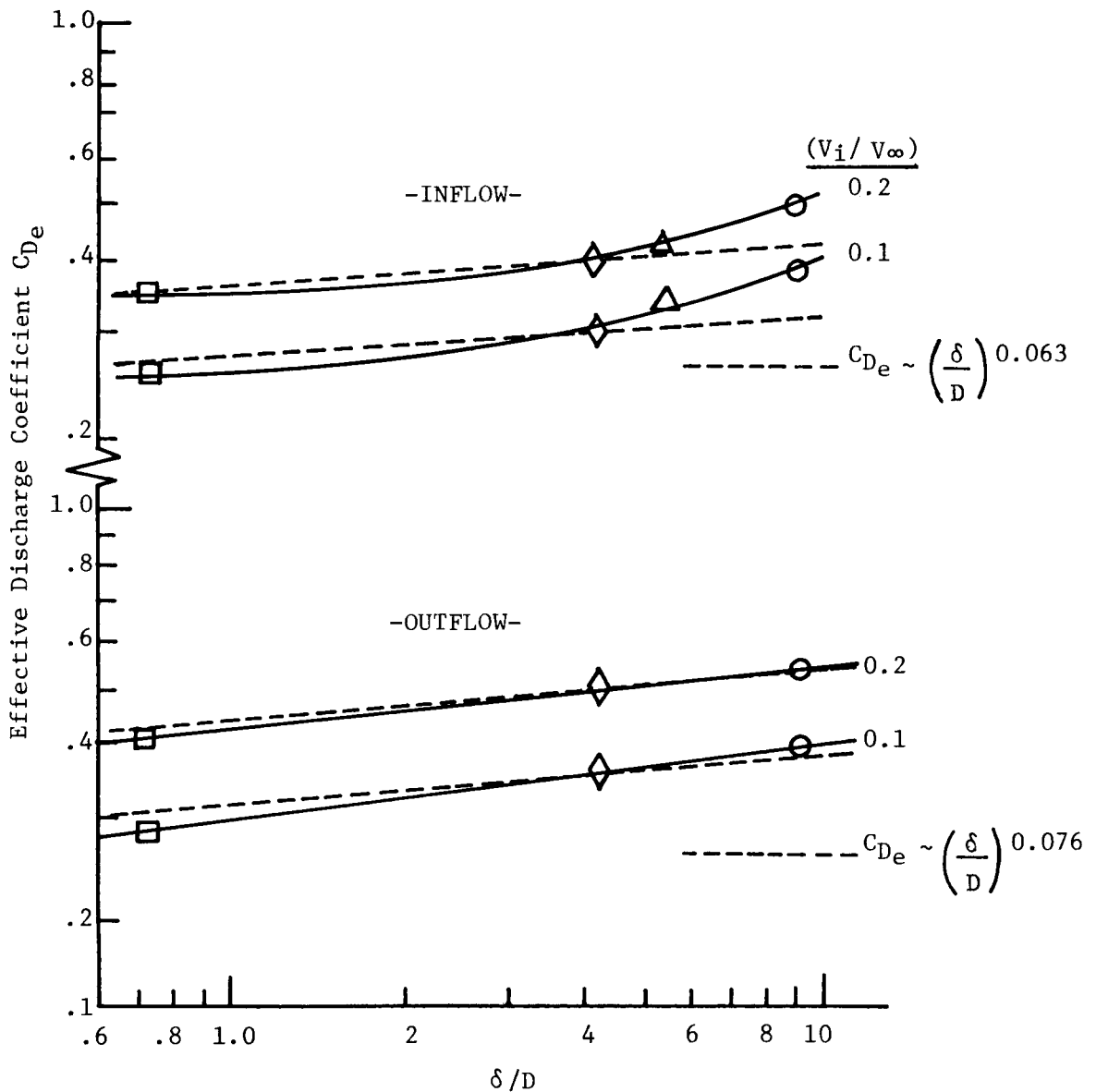


FIGURE 16. EFFECT OF BOUNDARY LAYER THICKNESS RATIO ( $\delta/D$ ) ON EFFECTIVE DISCHARGE COEFFICIENT ( $C_{De}$ )

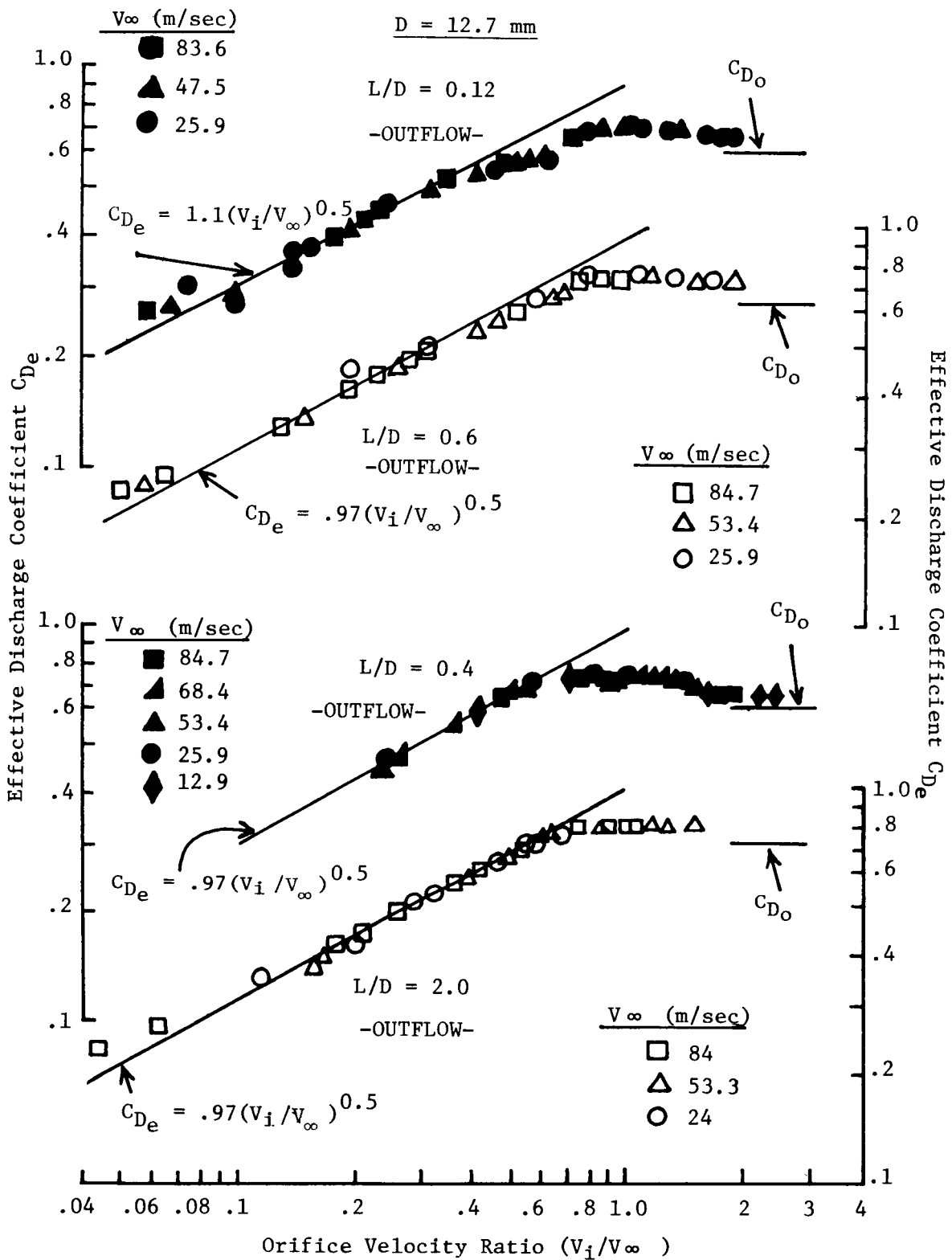


FIGURE 17. EFFECT OF LENGTH - DIAMETER ON CORRELATIONS OF OUTFLOW DATA IN GRAZING FLOW

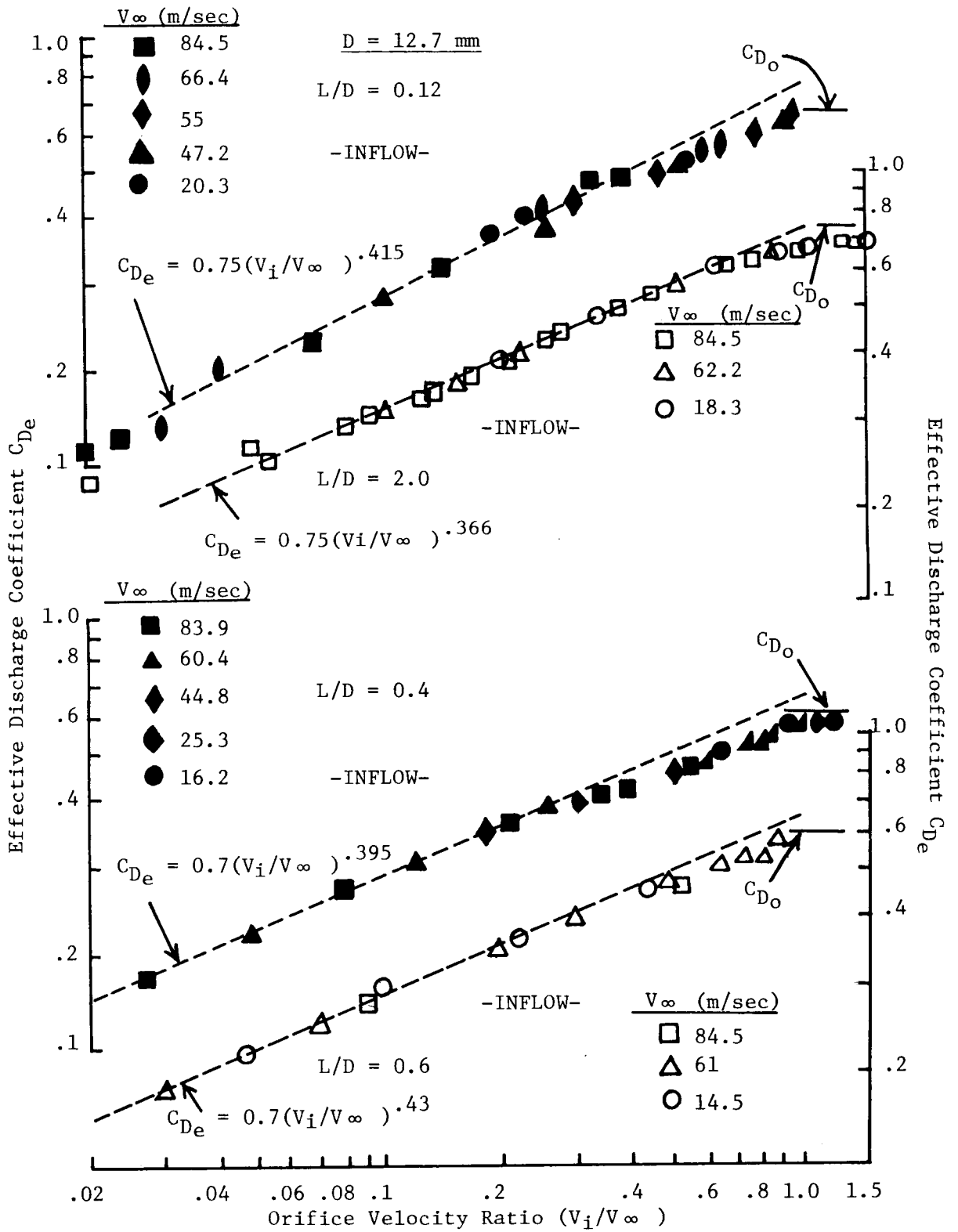


FIGURE 18. ORIFICE LENGTH - DIAMETER EFFECT ON CORRELATIONS OF INFLOW DATA IN GRAZING FLOW

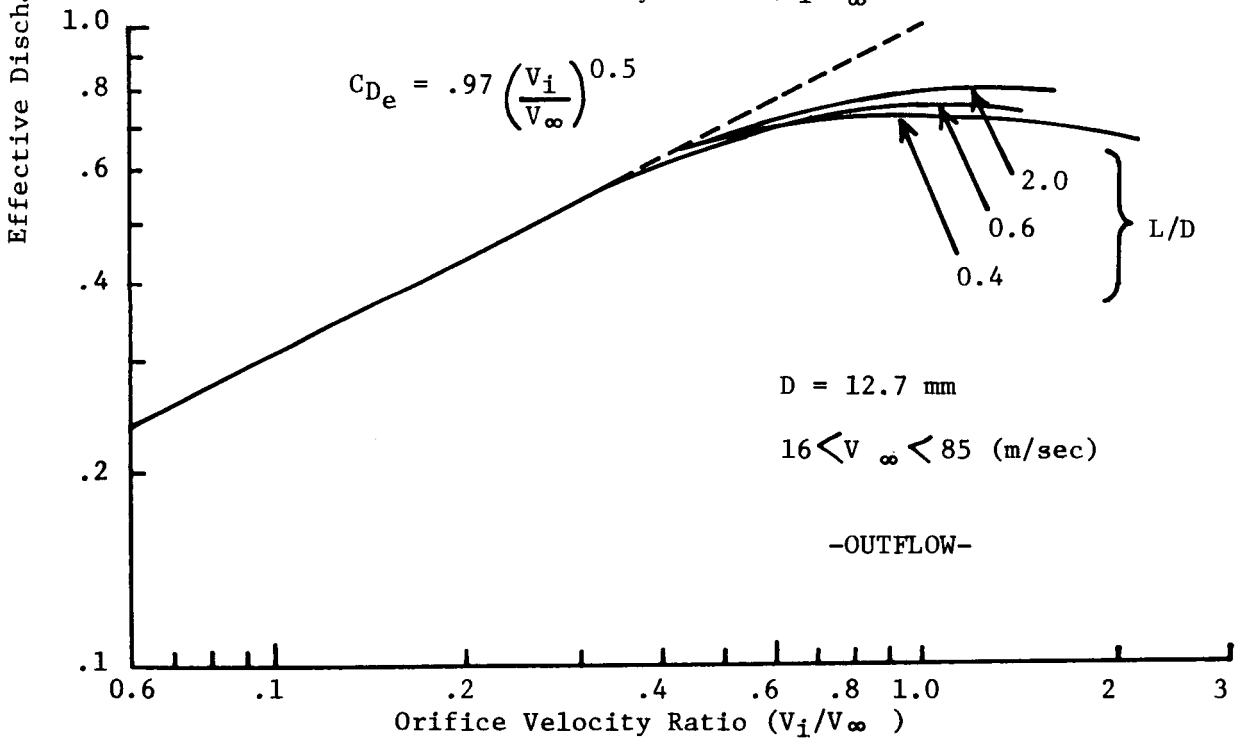
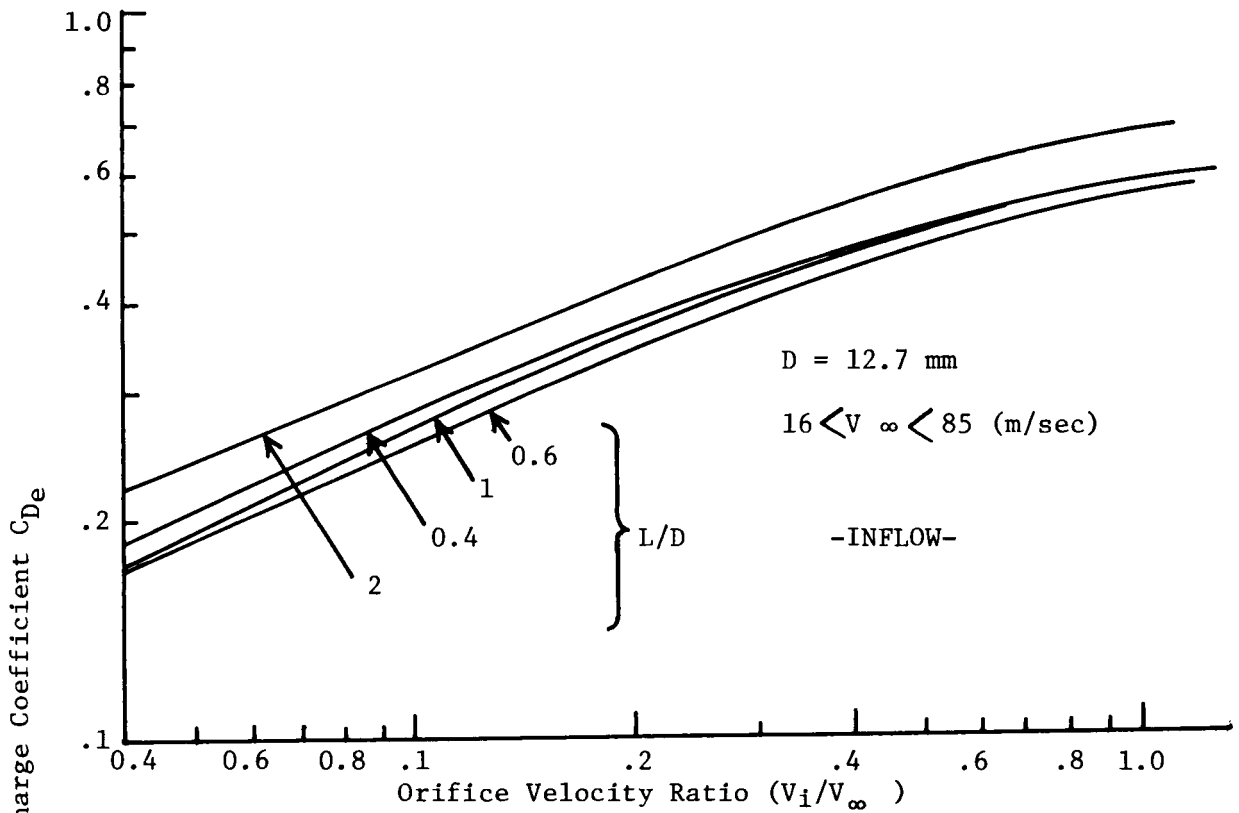


FIGURE 19. EFFECT OF LENGTH - DIAMETER RATIO ON EFFECTIVE DISCHARGE COEFFICIENT

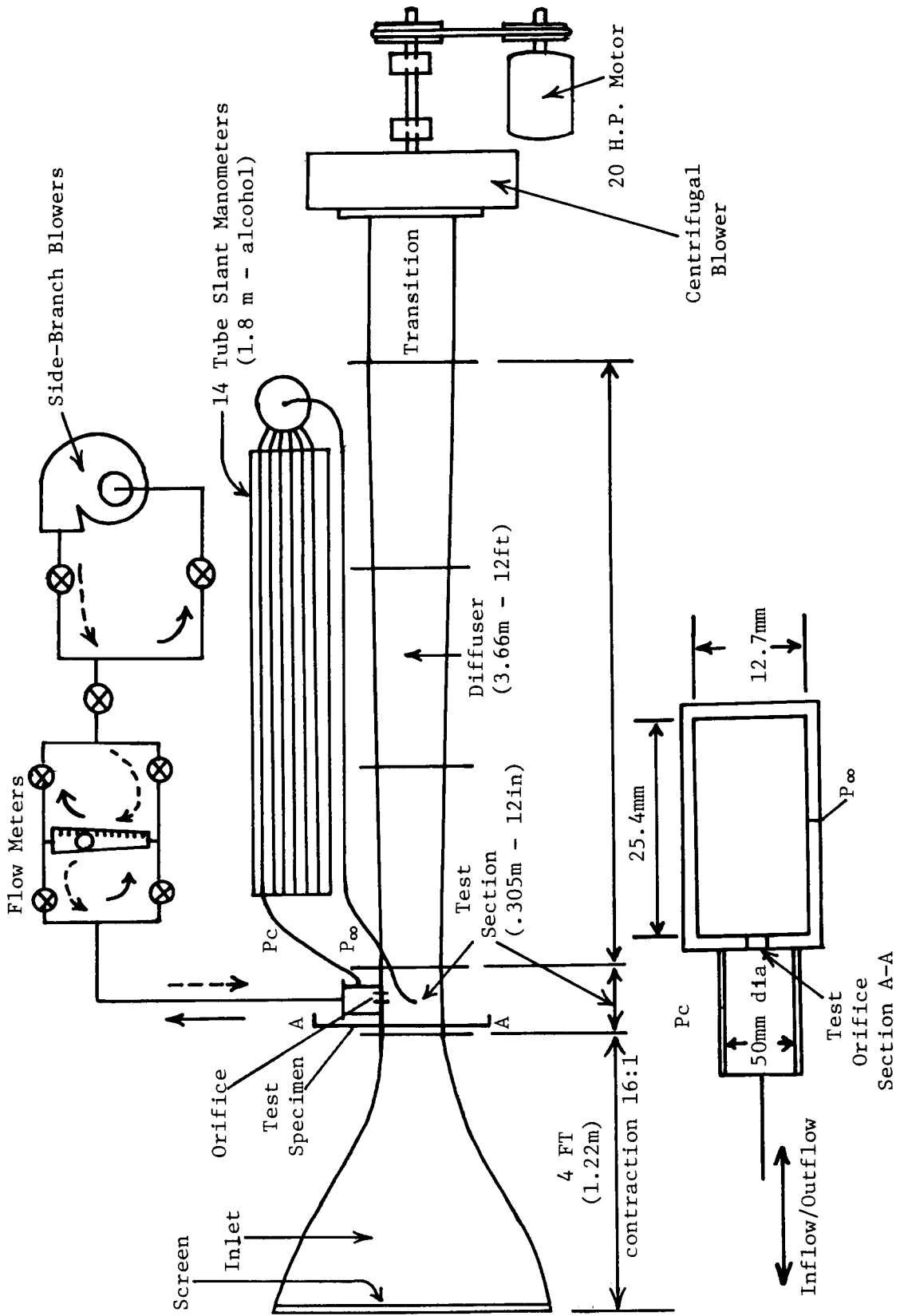


FIGURE B1. SCHEMATIC OF WIND TUNNEL

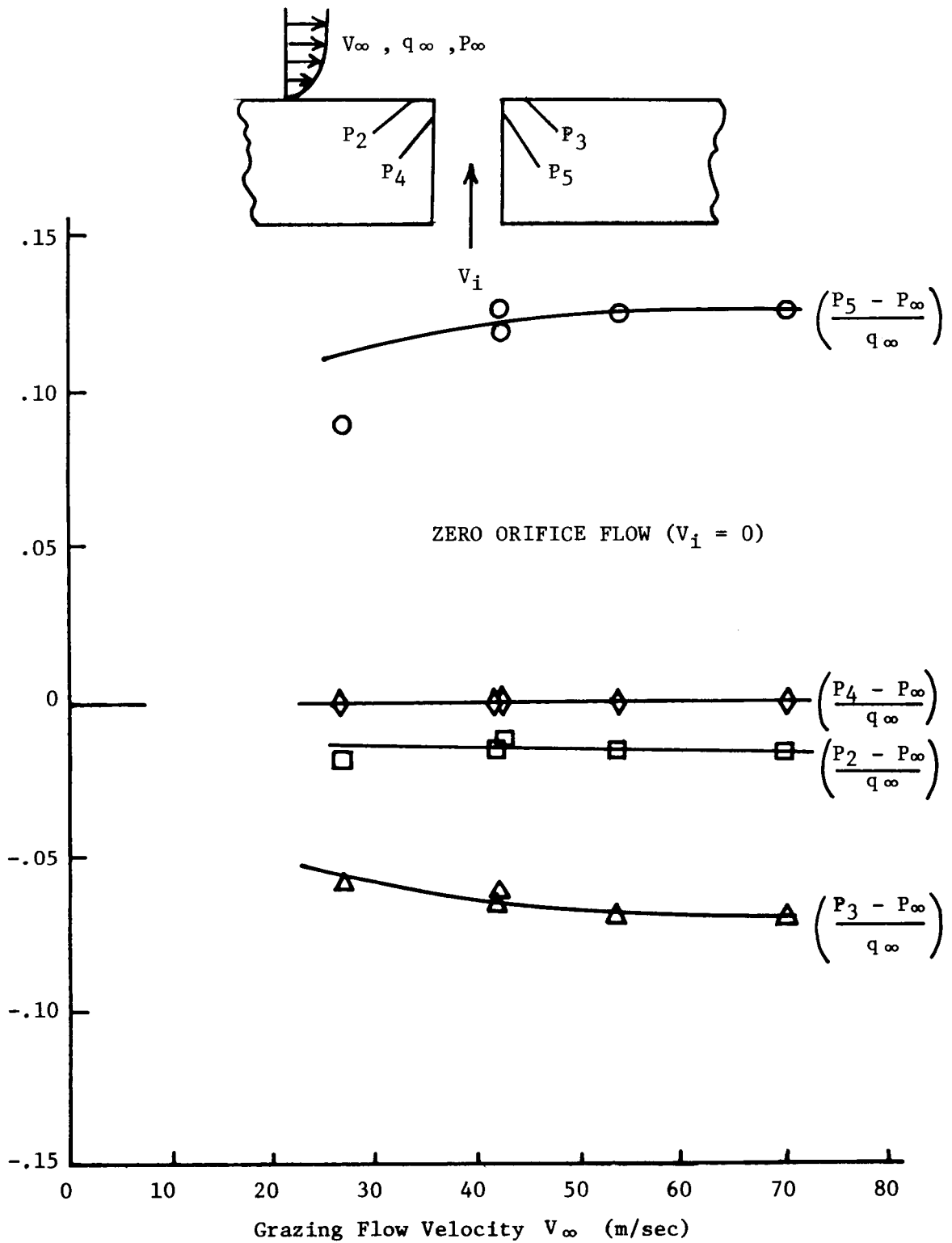


FIGURE C1. ORIFICE LIP STATIC PRESSURE VARIATION WITH GRAZING FLOW VELOCITY (FOR ZERO ORIFICE FLOW)

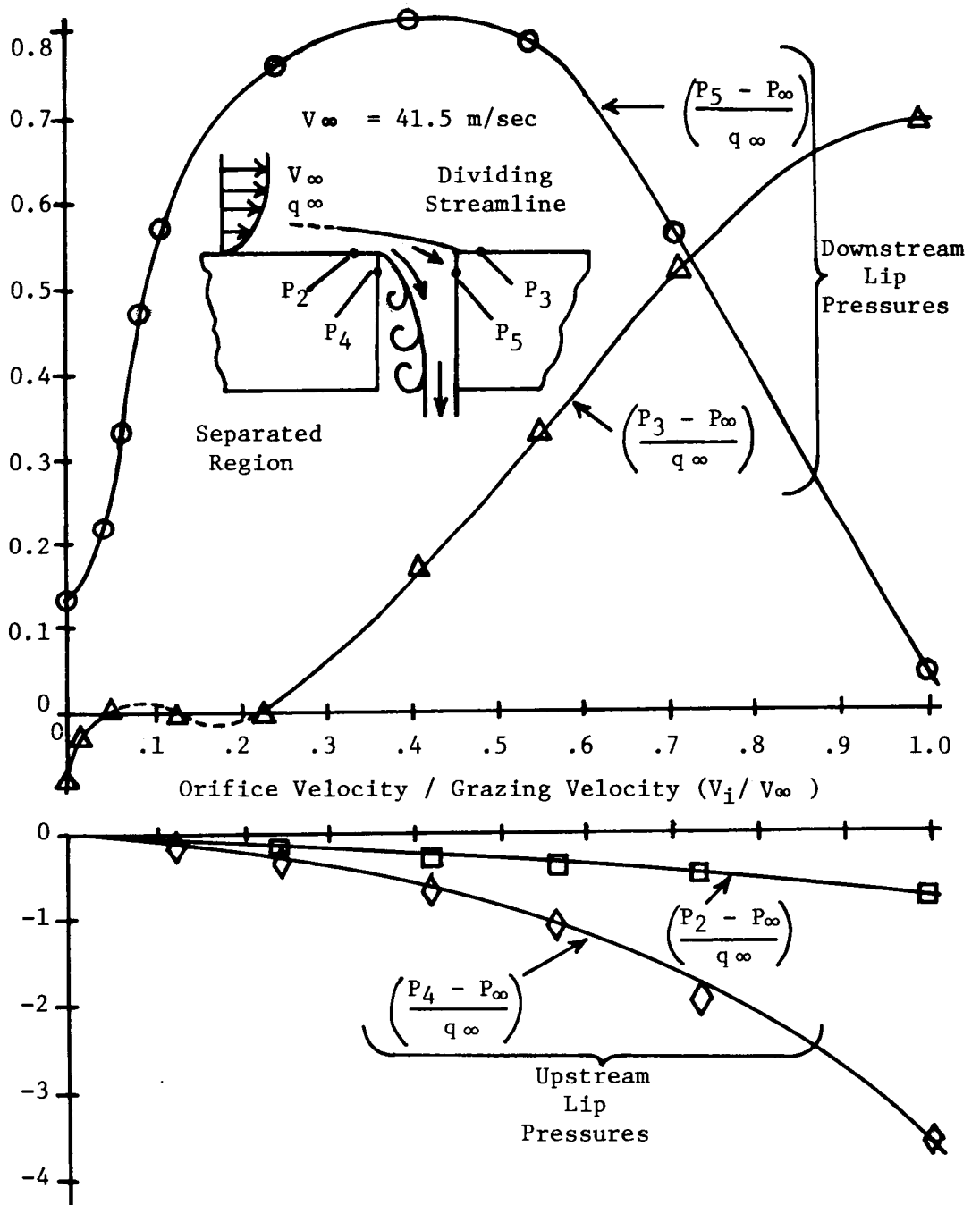


FIGURE C2. VARIATION IN ORIFICE LIP PRESSURES FOR INFLOW

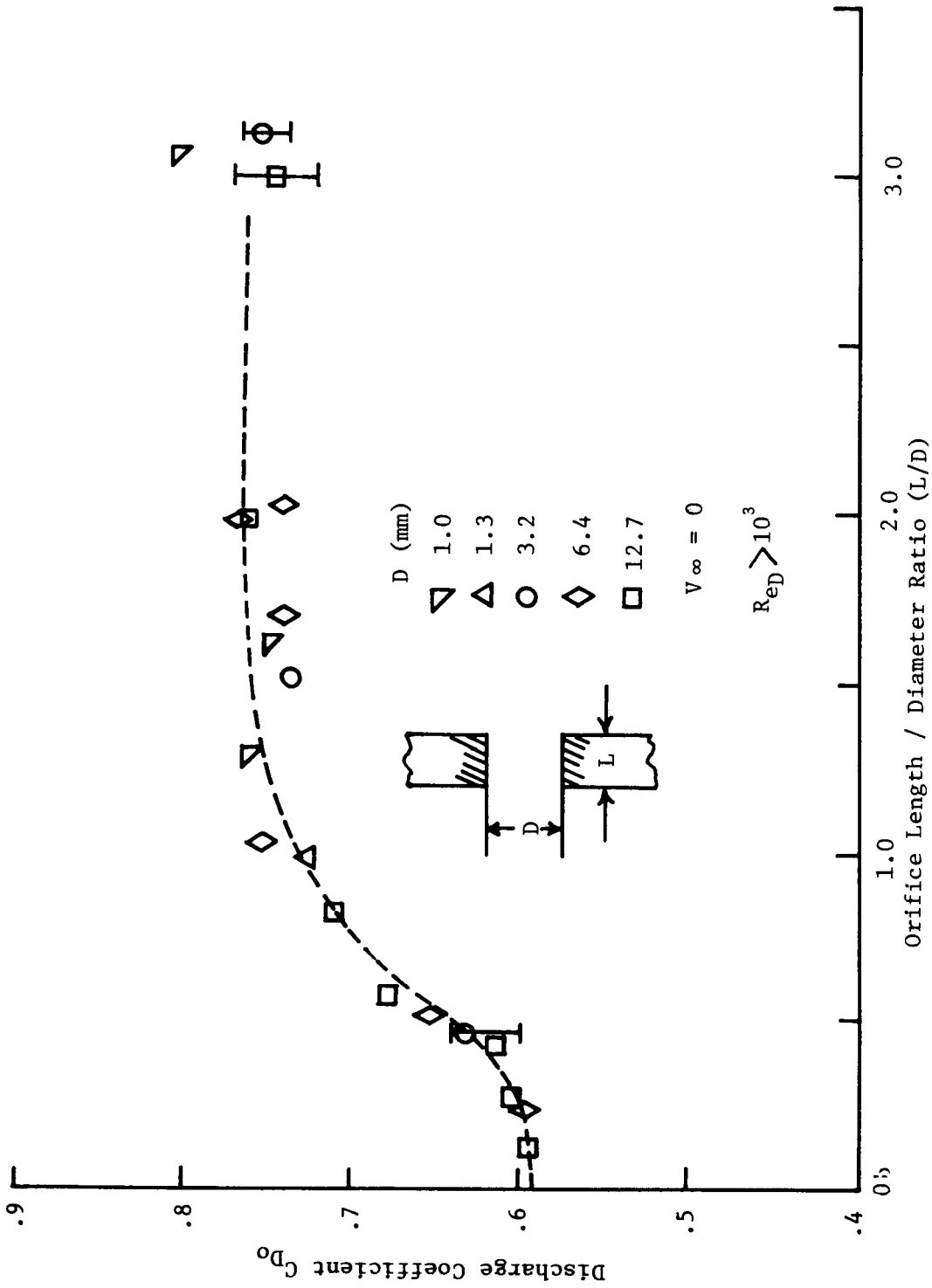


FIGURE E1. EFFECT OF L/D ON DISCHARGE COEFFICIENT OF SQUARE - EDGED ORIFICES IN NORMAL FLOW

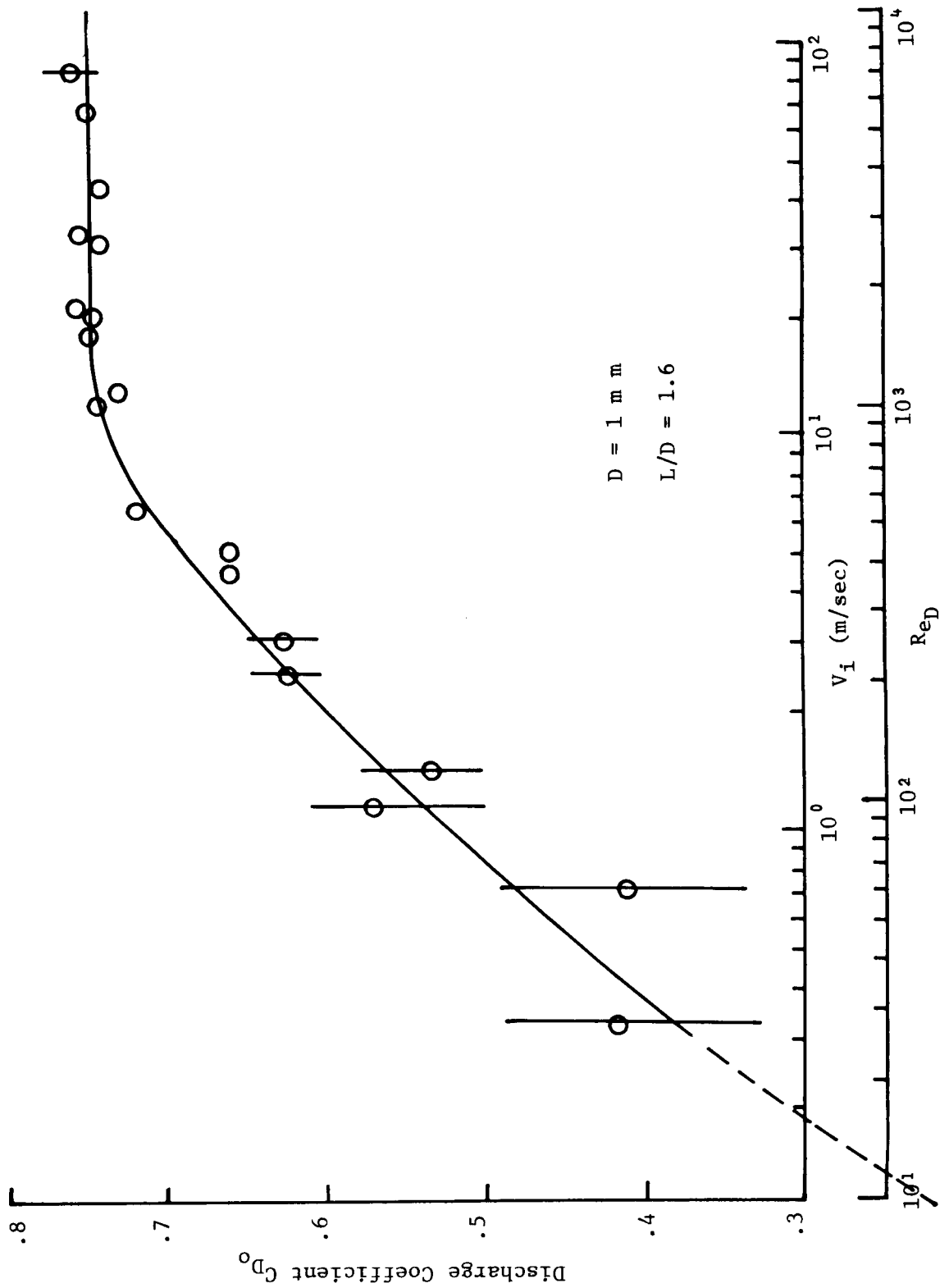


FIGURE E2. EFFECT OF LOW REYNOLDS NUMBER  $C_{D0}$